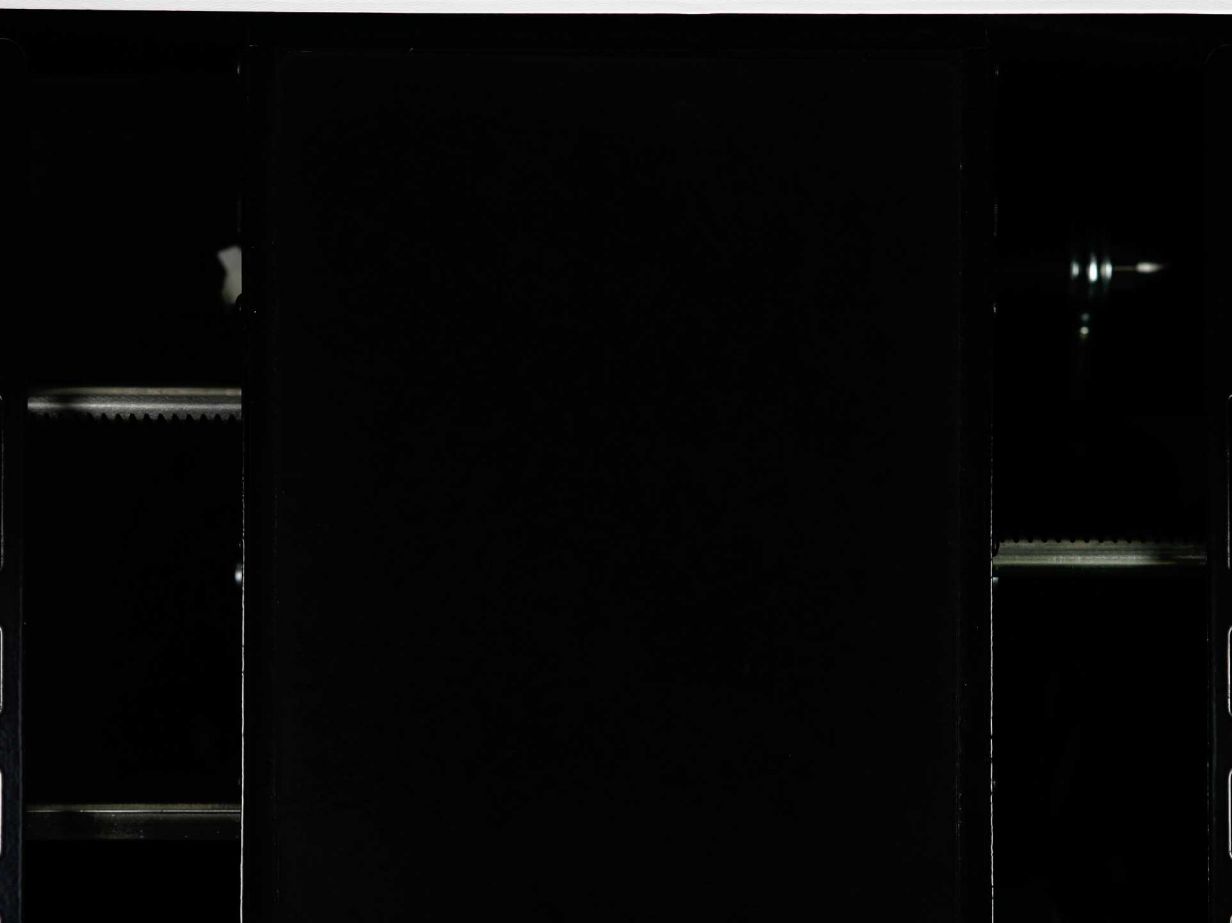

ANL/ESD/TM-72

Computation of Magnetic Forces on Moving Conductors by Using ELEKTRA and Other 3-D Computer Codes

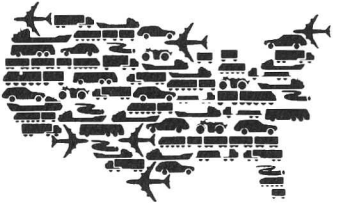

Center for Transportation Research
Argonne National Laboratory

Operated by The University of Chicago,
under Contract W-31-109-Eng-38, for the
United States Department of Energy

Argonne National Laboratory

Argonne National Laboratory, with facilities in the states of Illinois and Idaho, is owned by the United States Government, and operated by the University of Chicago under the provisions of a contract with the Department of Energy.

This technical memo is a product of Argonne's Energy Systems (ES) Division. For information on the division's scientific and engineering activities, contact:

Director, Energy Systems Division
Argonne National Laboratory
Argonne, Illinois 60439-4815
Telephone (708) 252-3724

Presented in this technical memo are preliminary results of ongoing work or work that is more limited in scope and depth than that described in formal reports issued by the ES Division.

Disclaimer

Reproduced directly from the best available copy.

Available to DOE and DOE contractors from the Office of Scientific and Technical Information, P.O. Box 62, Oak Ridge, TN 37831; prices available from (615) 576-8401.

Available to the public from the National Technical Information Service, U.S. Department of Commerce, 5285 Port Royal Road, Springfield, VA 22161.

ANL/ESD/TM-72

Computation of Magnetic Forces on Moving Conductors by Using ELEKTRA and Other 3-D Computer Codes

by Z. Wang, H.T. Coffey, and T. Mulcahy*

Center for Transportation Research, Energy Systems Division,
Argonne National Laboratory, 9700 South Cass Avenue, Argonne, Illinois 60439

August 1994

Work sponsored by U.S. Army Corps of Engineers and the Federal Railroad Administration, through interagency agreements E8691R001 and DTFR 53-91-X-00018, respectively, with the United States Department of Energy, and by Argonne National Laboratory

*Mulcahy is affiliated with Argonne's Energy Technology Division.

This report is printed on recycled paper.

Contents

Tables

Figures

Figures (Cont.)

Figures (Cont.)

Computation of Magnetic Forces on Moving Conductors by Using ELEKTRA and Other 3-D Computer Codes

by

Z. Wang, H. Coffey, and T. Mulcahy

Abstract

The finite-element computer code ELEKTRA is the only publicly available code known to us that is capable of solving 3-D eddy-current problems that entail the use of moving electrical conductors having finite dimensions. It is, therefore, expected to become a standard tool for the analysis of magnetic levitation (maglev) systems using sheet guideways. This study systematically evaluates the ELEKTRA code by comparing it with experimental data and "benchmark" solutions, as appropriate. In addition, alternatives to ELEKTRA were investigated, and a new computer code, based on an extension of the double-Fourier series analysis, was developed.

1 Introduction

Magnetic levitation (maglev) transportation systems have received considerable attention as a means of relieving both highway and air-traffic congestion with minimal environmental impact. The National Maglev Initiative was established to assess the potential of these systems in the United States. As a part of the National Maglev Initiative program, contracts were awarded for four maglev system concept definitions. Three of these systems could be analyzed by more-or-less standard means of analysis. The fourth, however, used a reaction plate of aluminum as part of the levitation system and required a nonstandard analysis. A Government Maglev System Assessment team was established to assess the technical viability of these concepts. The results and the supporting analyses for the magnetic calculations made by this team were evaluated by the maglev group at Argonne National Laboratory (ANL).

The velocity version of ELEKTRA is a finite-element computer code, developed by Vector Fields, Ltd., that is capable of solving three-dimensional (3-D) eddy-current problems with a moving conductor. As the only known publicly available code capable of solving these problems, it is likely to become a standard tool for the analysis of maglev systems. On the other hand, the ELEKTRA code is new and untested; it is important, therefore, that the code be systematically validated. Since the ELEKTRA code's use is complicated, formal training of users is necessary. (Training is available from Vector Fields, Ltd.)

The objectives of this report are (1) to validate solutions of the ELEKTRA code with experiments and known analytical solutions for different sizes of magnets over a wide velocity

range; (2) to check the code's ability to simulate full-scale, full-speed systems; and (3) to develop an alternative method as a contingency in case ELEKTRA proves unsatisfactory.

An analogous computer program, called MAGFORCE, was developed at ANL by H. Coffey. This program is based on a published Fourier transformation formulation (Coffey 1972). MAGFORCE was used to check and validate ELEKTRA calculations.

This report consists of seven sections.

Section 1, this section, outlines the coverage of the study.

Section 2 describes the comparison of ELEKTRA and MAGFORCE calculations with experimental data, measured by ANL staff, for a small-scale rectangular magnet suspended over a moving aluminum plate.

Section 3 demonstrates that ELEKTRA is capable of edge-effects analysis by simulating a small rectangular coil near the edge of the moving aluminum plate.

Section 4 details the numerical error introduced when calculating forces using very low velocity and then details corrective measures for avoiding the error.

Section 5 demonstrates that ELEKTRA is unable to simulate a large-scale, full-speed real maglev system unless a new algorithm is used, such as the upwinding technique.

Section 6 discusses other alternatives that might be used to calculate forces for continuous-sheet guideways. A new computer code, based on a double-Fourier series method, was developed at ANL, and results were compared with experimental data and MAGFORCE and ELEKTRA results.

Section 7 gives the conclusions reached on the basis of this study.

2 Validation of ELEKTRA with an Experimental Model

A simple laboratory model was used to validate the predictions of ELEKTRA at a small scale and low velocity. Figure 1 shows the configuration of the small-scale laboratory/computer simulation model. In these experiments, the forces were measured on a 50.8- × 25.4- × 6.35-mm permanent magnet suspended over a 1.2-m diameter, vertically mounted, rotating wheel wrapped with a 6061-T6 aluminum plate. The wheel and aluminum plate were rotated at different velocities for the experiment. The aluminum plate wrapped around the wheel is 6.35 mm thick and 101 mm wide. The magnet was suspended at different set distances over the moving plate.

The lift and drag forces, measured by Debora Yacobellis and Thomas Mulcahy, were compared with calculations made with ELEKTRA and MAGFORCE. MAGFORCE, which is very fast, has been found to be quite reliable in calculating the forces experienced by magnets over infinitely wide conducting sheets of variable thickness; however, it is not capable of computing the effects of finite widths. MAGFORCE serves as a good benchmark for verifying the calculations of ELEKTRA, which is slow but capable of performing finite-width calculations and working with more complex model geometries.

For all experiments, the Peclet number ($p = vh\mu\sigma/2<1$) must be satisfied. (In calculating the Peclet number, σ is plate conductivity, v is plate velocity, μ is plate permeability, and h is the average element length [mesh size] in the direction of velocity.) The Peclet number must be smaller than 1 to avoid oscillation in the numerical computations.

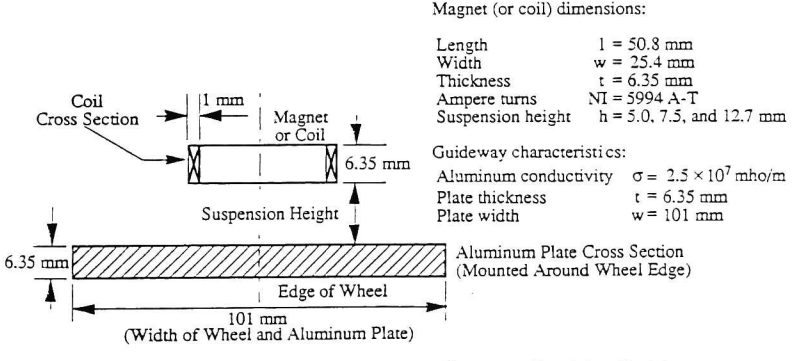

FIGURE 1 Configuration of a Small-Scale Laboratory/Computer Simulation Model (cross section)

Since neither MAGFORCE nor ELEKTRA simulates a permanent magnet directly, an equivalent coil has to be used in the computer calculations. In order to simulate the permanent magnet used for the experiments, the equivalent ampere-turns of the coil must be determined. One way to determine the ampere-turns is to compare the amplitude and shape of the magnetic field in the gap between the permanent magnet and the aluminum conductor plate. Using this technique, a coil equivalent to the magnet used in the experiments would have 5,994 ampere-turns (NI). The outer dimensions of the coil used in ELEKTRA (and MAGFORCE) correspond exactly to the outer dimensions of the permanent magnet used in the experiment; the coil cross section is 1-mm wide by 6.35-mm high.

When constructing the coil mesh for the computer simulation, the mesh distribution around and inside the coil should be made as fine as possible to obtain more accurate force computations. Since the magnet or coil is positioned at the center of the aluminum plate, the symmetrical condition can be used. This means only half the space needs to be meshed and calculated. The total number of nodes for the half-space is around 16,000. Computer computation time for a specific velocity is normally around 2–3 h.

Figures 2 through 4 show the lift and drag forces vs. velocity calculated for suspension heights of 5, 7.5, and 12.7 mm. Experimental results are plotted along with ELEKTRA and MAGFORCE calculations. Both MAGFORCE and ELEKTRA calculations agree closely with the experimental data. Calculated forces for a 12.7-mm suspension height, however, match the experimental data better than those for a 5-mm suspension height. The reason may be that in the experiments the permanent magnet is partially demagnetized. This demagnetization reduces the lift and drag forces. When the magnet is closer to the aluminum plate, a greater magnetic force is created. The stronger the magnetic force between the magnet and the plate, the stronger the demagnetization effect becomes. However, neither MAGFORCE nor ELEKTRA considers this effect.

When the velocity was reduced to 2 m/s, the lift forces calculated from ELEKTRA appear slightly negative, as shown in Figures 2 and 3. This numerical error is caused by the method used to compute the net force — the force is calculated as the small differences in large numbers. In order to obtain accurate results for very low speeds, special measures must be taken, as discussed later in Section 4.

To test ELEKTRA symmetrically, the number of nodes was gradually increased for one case (suspension height = 12.7 mm and velocity = 20 m/s) to see how the number of nodes affects the results. The comparison of the different mesh nodes for the ELEKTRA code is shown in Table 1. In Table 1, case 1 with 16,324 nodes was taken as a reference and all other cases were compared with it. Table 1 shows that the more nodes, the more accurate the results. The trade-off is that a higher number of nodes requires more computing time.

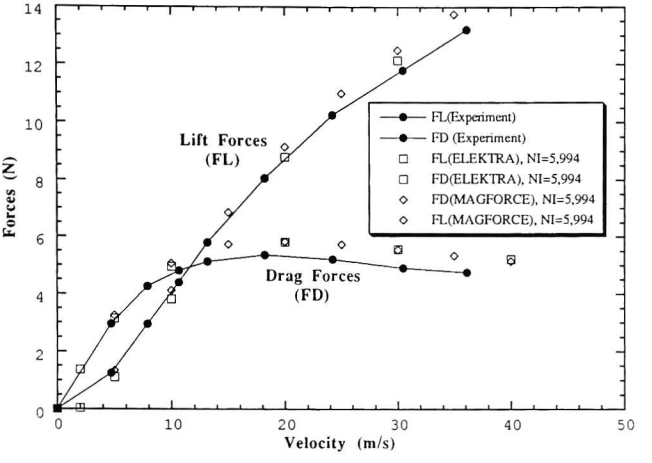

FIGURE 2 Forces on a 50.8- × 25.4- × 6.35-mm Magnet Suspended 5.0 mm over a Moving 6.35-mm-Thick Aluminum Plate

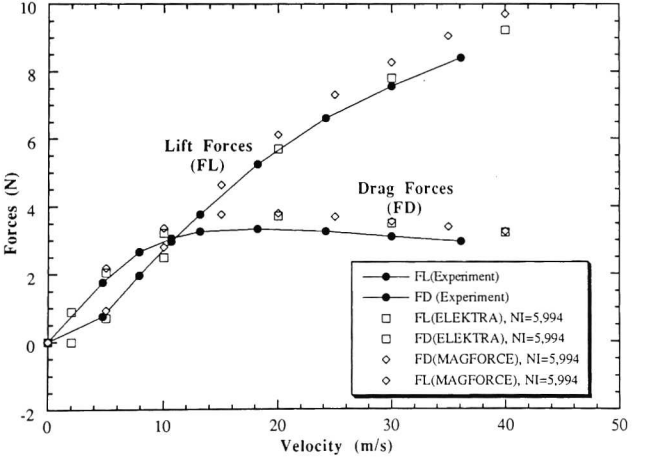

FIGURE 3 Forces on a 50.8- × 25.4- × 6.35-mm Magnet Suspended 7.5 mm over a Moving 6.35-mm-Thick Aluminum Plate

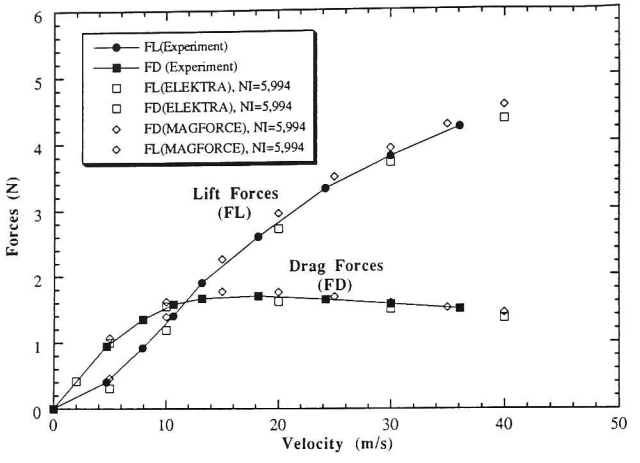

FIGURE 4 Forces on a 50.8- × 25.4- × 6.35-mm Magnet Suspended 12.7 mm over a Moving 6.35-mm-Thick Aluminum Plate

TABLE 1 Comparison of Different Mesh Nodes for the ELEKTRA Code

No. of Nodes	Lift Force (N)	Drag Force (N)	Lift Force Difference (%)	Drag Force Difference (%)	Computing Time (min)
16,324	2.413	1.566	0	0	112
11,289	2.309	1.559	4.3	-0.4	74
6,390	2.265	1.606	6.1	2.55	30
4,950	2.269	1.821	5.97	16.28	21

In summary, as long as the Peclet number is satisfied, and the velocity is not too low, the velocity version of ELEKTRA works very well. When the velocity is below 5 m/s, a numerical error in the lift force often occurs unless special measures, as discussed in Section 4, are taken. Velocity between 5 and 10 m/s may also cause problems. Velocities greater than 10 m/s work well in the ELEKTRA program.

3 ELEKTRA: Applied to Edge-Effects Analysis

As shown in Section 2, ELEKTRA worked very well (except at very low velocity) for a small laboratory model. This section presents the results obtained by using ELEKTRA to calculate the forces on a small rectangular coil near the edge of a moving aluminum plate. J. R. Hull conducted preliminary comparisons of this type in 1992, using rather coarse computation mesh sizes (Hull 1992). Expanding on this work, the mesh distributions were optimized and more nodes were added for more quantitative testing.

The geometry of the model and other information is the same as that presented in Section 2. The equivalent ampere-turns (NI) for this particular magnet was calculated to be 5,715. The gap (h) between the bottom of the magnet (coil) and the top surface of the aluminum plate is 12.7 mm; the distance of the magnet (coil) from the edge of the aluminum plate is H*.

Three different values of H* have been simulated: H* = 12.7 mm (more than 100% overlap), H* = 0 mm (100% overlap), and H* = -12.7 mm (50% overlap). See Figures 5 through 7. The total number of nodes is about 15,000, and the average number of iterations to achieve convergence is around 300–500 at low velocities (10–20 m/s) and 800–1,000 at high velocities (30–40 m/s). Around 3–4 h of computation is required for each velocity. The calculated and experimental lift, drag, and guidance forces (shown in Figures 5 through 7) are in reasonable agreement, considering the uncertainty in the parameters used (especially the conductivity of the aluminum plate and the equivalent-current density in the magnet). Note that guidance forces are created since the magnet (coil) is not located symmetrically over the aluminum plate. The agreement between calculated and experimental results, as shown in Figure 8, can be improved further by increasing the number of nodes (beyond 18,000 nodes) in the coil mesh. This is to be expected because at higher velocities the skin depth decreases, resulting in a steeper gradient in the magnetic field and requiring more nodes to accurately describe the field variation with magnet position on the plate.

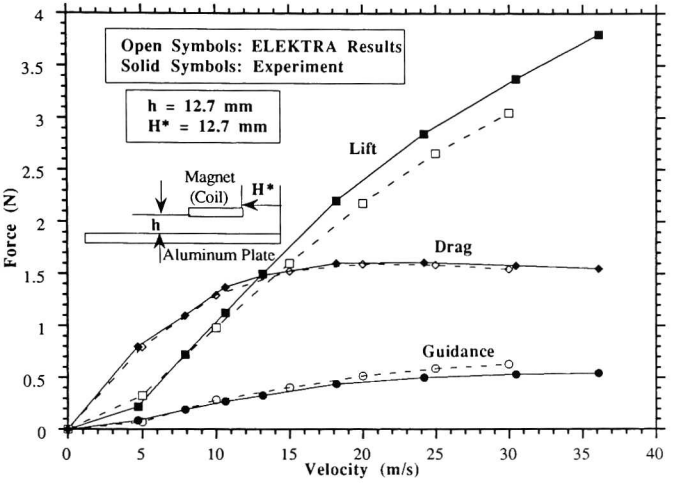

FIGURE 5 Force on a 50.8- × 25.4- × 6.35-mm Magnet Suspended over a Moving 6.35-mm-Thick Aluminum Plate, 15,000 Nodes for ELEKTRA; H* = 12.7 mm

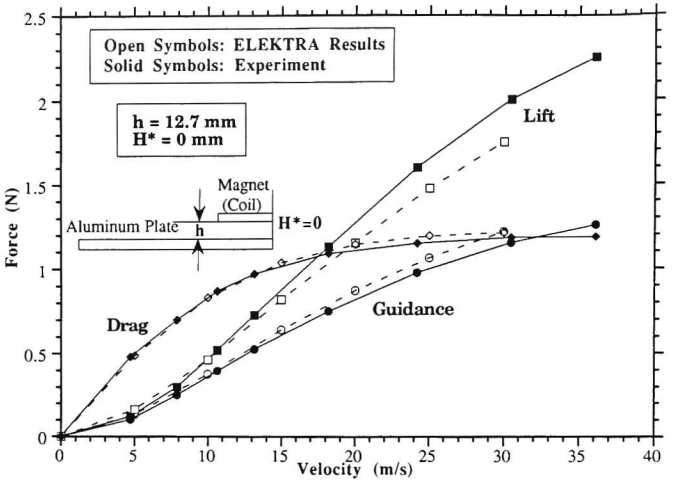

FIGURE 6 Force on a 50.8- × 25.4- × 6.35-mm Magnet Suspended over a Moving 6.35-mm-Thick Aluminum Plate, 15,000 Nodes for ELEKTRA; H^* = 0 mm

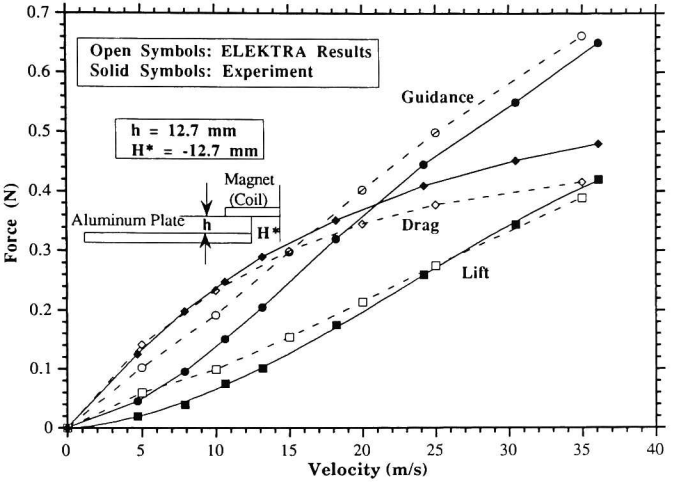

FIGURE 7 Force on a 50.8- × 25.4- × 6.35-mm Magnet Suspended over a Moving 6.35-mm-Thick Aluminum Plate, 15,000 Nodes for ELEKTRA; $H^* = -12.7$ mm

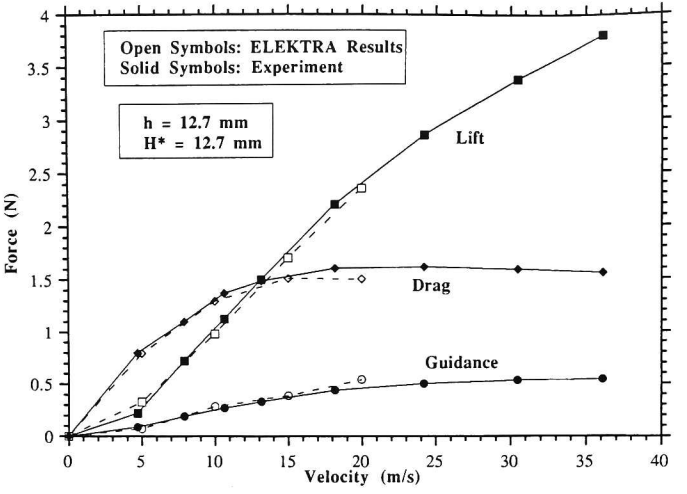

FIGURE 8 Force on a 50.8- × 25.4- × 6.35-mm Magnet Suspended over a Moving 6.35-mm-Thick Aluminum Plate, 18,000 Nodes for ELEKTRA; H* = 12.7 mm

4 ELEKTRA: Analysis at Very Low Velocities

In Sections 2 and 3 it was shown that ELEKTRA works well for small-scale laboratory models. In this section ELEKTRA will be evaluated for medium-size models. The geometry of the coil in the simulated test model (shown in Figure 9) is the same as that used in the Magneplane design (Coffey et al. 1992), but it is reduced in size by a factor of four. The coil size is $570 \times 110 \times 10$ mm; the aluminum plate is 1,600-mm wide and 20-mm thick, with conductivity of $\sigma = 2.5 \times 10^7$. In order to satisfy the Peclet number, the maximum velocity that ELEKTRA can simulate is 5 m/s if the number of nodes is to remain within our computer's capacity. Problems were encountered when the velocity was reduced to 2 m/s.

Three coil mesh discretizations were set up, as shown in Figure 10. These mesh discretizations are almost the same except that in the region indicated by an arrow; the number of subdivisions is 5, 8, and 10 for cases 1, 2, and 3, respectively. The total number of mesh elements (nodes) in these three mesh models is 16,458, 21,879, and 22,113, for cases 1, 2, and 3, respectively. These slight differences in the number of nodes were not expected to change the overall results significantly. However, big differences in the computed lift force were found, as shown in Table 2.

The eddy currents in the aluminum plate were calculated and plotted for the three cases shown in Figure 11. There was no perceptible difference. However, Figure 12 shows that B_x at the plane y = 50 mm (which is the center plane of the coil) is different in each of these three cases. B_x causes large differences in the lift force calculated by $\int_v \tilde{J} \times \tilde{B}\, dv$. The coil components C and D (shown in Figure 9) always produce a *repulsive force*. For coil components A and B (shown in Figure 9) in which the current is flowing in the z-direction (the velocity direction), the product of B_x times current (J) produces the *lift force*. The sign of B_x changes along the velocity direction (z), while the direction of the current remains the same. Therefore, the front part (velocity direction) of these two elements (A and B) produces a *repulsive force* and the rear part of these two elements produces an *attractive force*. The net force is the difference between the repulsive and attractive forces; normally the repulsive force is greater. These two large-force cancellations may cause a big difference in the force results. Figure 13 shows the lift-force distributions along the coil for cases 1–3 and 6. The values in parentheses were obtained by different commands in the post processor.

When different potentials in the ELEKTRA system are assigned, completely different answers result, although both are used correctly according to the menu. According to the menu, three kinds of potentials are defined: vector, reduced scalar, and total scalar. The *vector potential* is for conducting-material-carrying eddy currents. The *reduced scalar potential* can be used for any material and must be applied to volumes which contain source conductors. The *total scalar potential* can be used for air and any nonconducting material.

The total scalar, reduced scalar, and vector potentials for cases 1–3 are shown in Figure 14; force results for cases 1 and 3 are shown in Table 3. Some regions were changed

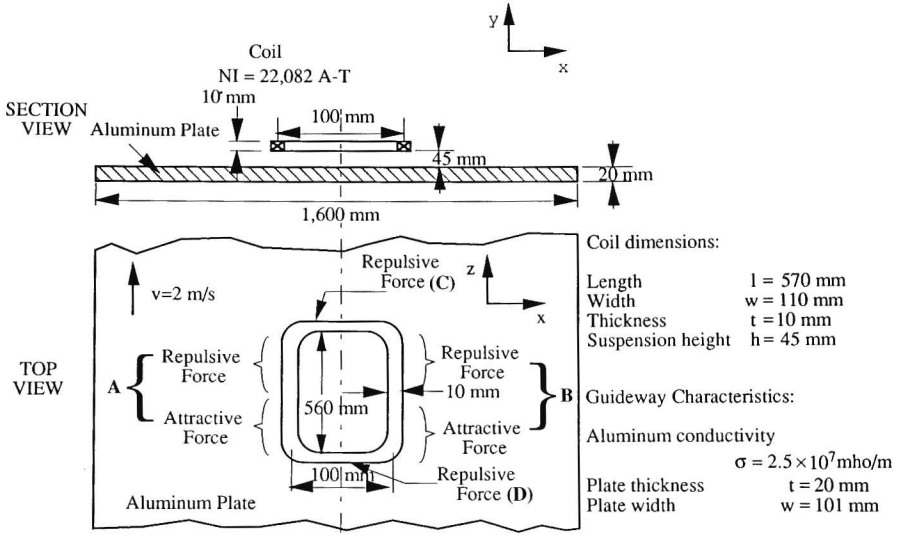

FIGURE 9 Configuration of the Simulated Test Model

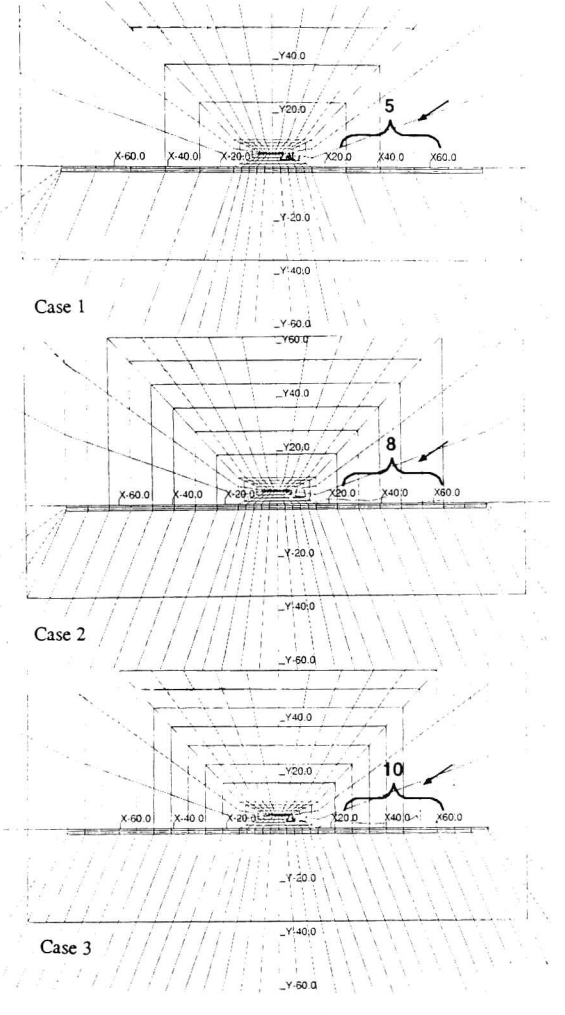

FIGURE 10 Coil Mesh Distributions for Cases 1–3

TABLE 2 Comparison of Forces for Three Mesh Models

Case	No. of Nodes	Lift Force (N)	Drag Force(N)
1	16,458	42.1674	41.8236
2	21,879	6.4884	40.6935
3	22,113	-5.1105	40.5227

from total scalar to reduced scalar potential, as shown in Figure 15 where cases 4 and 5 were calculated. (In Figure 15 the mesh distribution of case 4 is the same as the that of case 1, and that of case 5 is the same as that of case 3.) The force results illustrated in Table 3 seem to depend greatly on the scalar potential definition. As shown in both Tables 2 and 3, inconsistent results were obtained for the lift force.

Lift force problems were reported to the ELEKTRA vendor who studied the case and concluded that the problem resulted from taking the difference between two large forces. In the post processor, we usually set FIEL = NODAL and COIL = INTE (referred to as NODAL/INTE) to recovery fields. When the velocity is very low, the FIEL = NODAL representation is not sufficiently accurate and large errors will occur. Therefore, the vendor suggested that we set FIEL = INTE and COIL = INTE (referred to as INTE/INTE) to obtain the best results for the five cases (1–5). Different mesh setups were tested following their suggestion. Consistent results were obtained with the command "set FIEL = INTE , COIL = INTE," but the forces are more than 10 times larger than expected. This problem was again reported to the vendor who finally realized that there was a real bug in the post processor using FIEL = INTE. A factor of 4π was omitted when evaluating the fields from the eddy currents. The new version of the program, using FIEL = INTE and COIL = INTE, resulted in consistent lift forces for the five cases. However, the ELEKTRA results were still about 20% larger than the MAGFORCE results, as indicated in Table 4.

Finally, an even finer mesh distribution (case 6) was designed. Considering the symmetric condition, the number of nodes for the half space was 17,325. The lift force in this case closely matched that of MAGFORCE, as shown in Table 4. The force distribution along the coil for case 6 is shown in Figure 13.

In summary, when the velocity is high, greater than 10 m/s, both the commands NODAL/INTE and INTE/INTE work well. When the velocity is very low, under 5 m/s, only INTE/INTE gives the correct results. The mesh distribution should be very fine for very low-velocity cases.

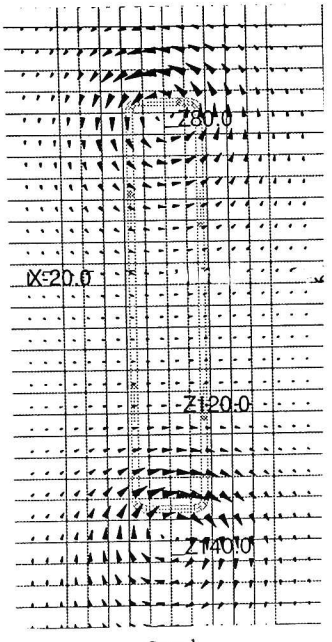

Case 1

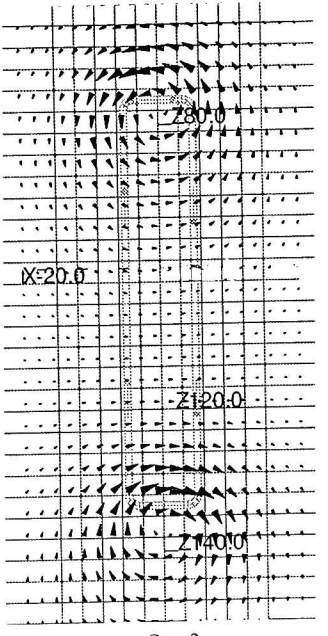

Case 2

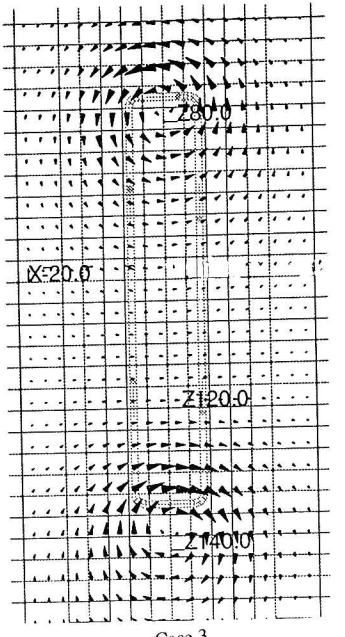

Case 3

FIGURE 11 Eddy Current Loops for Cases 1–3

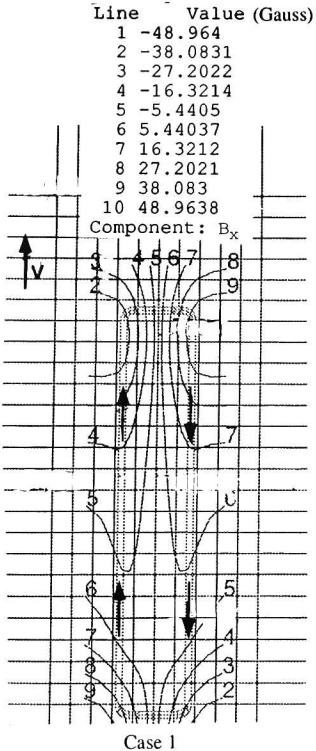

Case 1

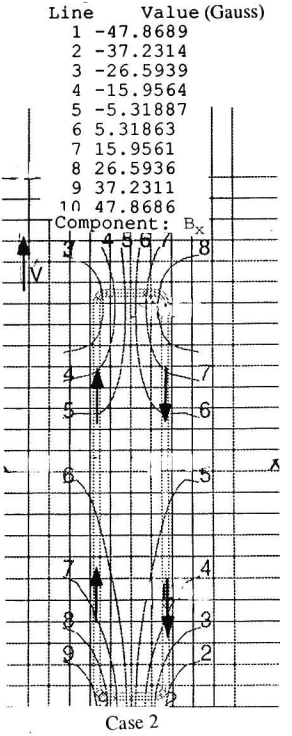

Case 2

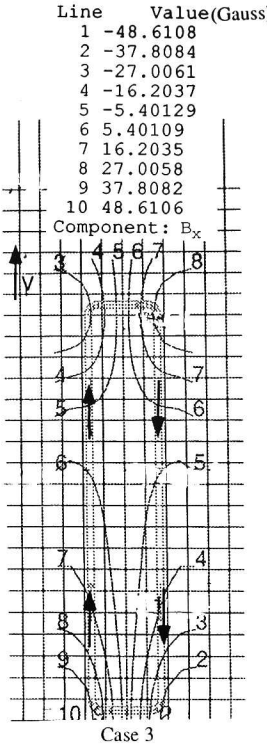

Case 3

FIGURE 12 Contours of Equal B_x on the Plane y = 50 mm for Cases 1–3

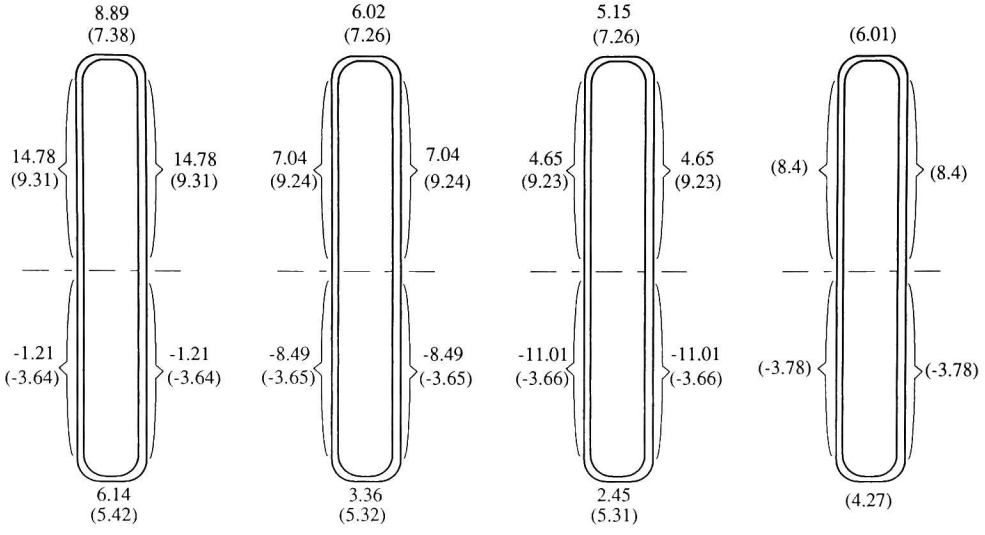

FIGURE 13 Lift-Force Distribution along the Coil at Low Velocity (v = 2 m/s) for Cases 1–3 and 6

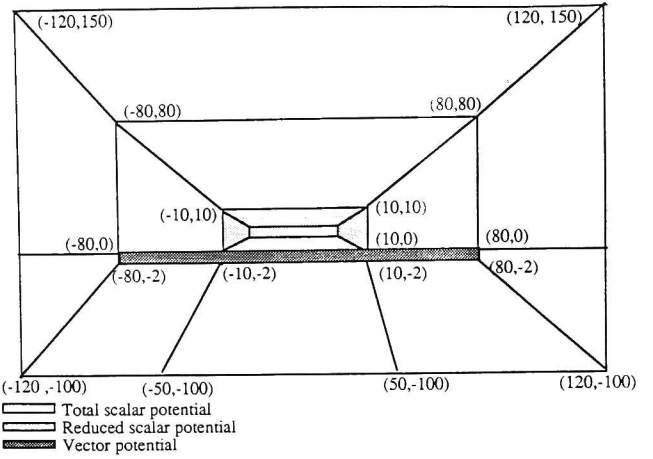

FIGURE 14 Potential Definitions for Cases 1–3

TABLE 3 Comparison of Forces for Different Scalar Potential Definitions

Case	No. of Nodes	Lift Force (N)	Drag Force (N)	Potential Definition
1	16,458	42.1674	41.8236	Reduced scalar area (Figure 14)
3	22,113	-5.1105	40.5227	Reduced scalar area (Figure 14)
4	16,458	-42.5561	41.1706	Reduced scalar area (Figure 15)
5	22,113	-40.2339	40.2824	Reduced scalar area (Figure 15)

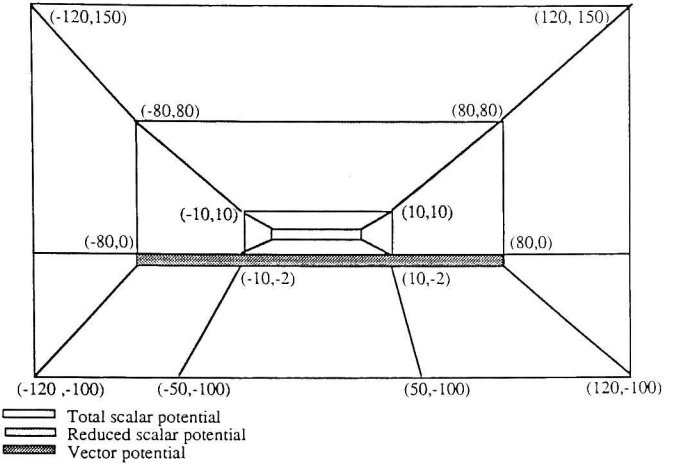

FIGURE 15 Potential Definitions for Cases 4 and 5

TABLE 4 Comparison of ELEKTRA Program with MAGFORCE Program

Computer Program	No. of Nodes	Lift Force (N)	Drag Force (N)
ELEKTRA Cases			
1	16,458	24.15	34.18
2	21,879	23.78	33.99
3	22,113	23.70	33.94
4	16,458	23.58	33.95
5	22,113	23.81	34.22
6	34,650	19.51	32.18
MAGFORCE	-	18.35	32.26

5 ELEKTRA: Unable to Simulate Large-Scale Maglev Systems

ELEKTRA can, in principle, solve various 3-D eddy-current problems. However, when it was used to calculate the forces for the Magneplane system, computational problems (numerical instability) were encountered. The reason is that the velocity option of ELEKTRA requires the Peclet number to be smaller than 1 to avoid oscillations in the solution, i.e., numerical instability. In designing meshes for larger systems, such as the Magneplane system (a practical maglev size), it was discovered that the mesh criterion imposed a very difficult condition. A mesh spacing of 6.5 mm is required for velocities of only 10 m/s. A realistic 3-D mesh, therefore, would require around 1.5×10^6 nodes, about 50 times the capacity of the Sun Sparc computer used in the calculations. An order of magnitude of additional points would be required for calculation at full speed. These problems were brought to the attention of the ELEKTRA developer, who designed (and recently released) an alternative algorithm that may avoid the numerical instability, thus allowing work with a high-velocity, full-scale maglev system.

6 Other Methods for Solving 3-D Eddy-Current Problems with Moving Conductors

6.1 Literature Search

The new, expanded velocity version of the ELEKTRA code, which is designed to solve large-scale sheet-guideway problems at high speeds, was not available at the time this study was made. Therefore, we did a literature search to see if other alternatives could resolve the problems.

Four approaches were identified:

- Double-Fourier Series Method
- T-Method
- EDDYCUFF Computer Code
- Finite-Element Method with Upwinding

The four approaches solve essentially the same problems, such as transverse edge-effect analysis. The double-Fourier series method, T-method, and EDDYCUFF computer code have the same approximation, i.e., the thickness of the sheet guideway is ignored. The finite-element method with upwinding (new high-velocity version of ELEKTRA), of course, uses finite elements in the calculations.

6.1.1 Double-Fourier Series Method

The double-Fourier series method was used earlier to analyze sheet-guideway problems (Ooi and Eastham 1975; Ooi 1975). In this method, the function can be formulated for two dimensions. An infinite number of parallel rows of infinitely long, infinitesimally thin strip guideways of finite width (d) were modeled. Rectangular superconductor coils (l long and w wide) were arrayed periodically along the strip guideway, as shown in Figure 16. The Fourier period was L in the velocity direction (x) and W in the transverse direction (z). L and W could be chosen large enough so that each coil was considered to be electromagnetically isolated. The basic idea of this approach was to model the coil as a double-Fourier series, then find an expression for the eddy currents in the sheet guideway, and finally apply the Lorentz Force Law $J \times B$ to the volume of the guideway to obtain the lift and drag forces (Ooi and Eastham 1975). (See Appendix A for detailed information on the derivation of the eddy current for the sheet guideway.)

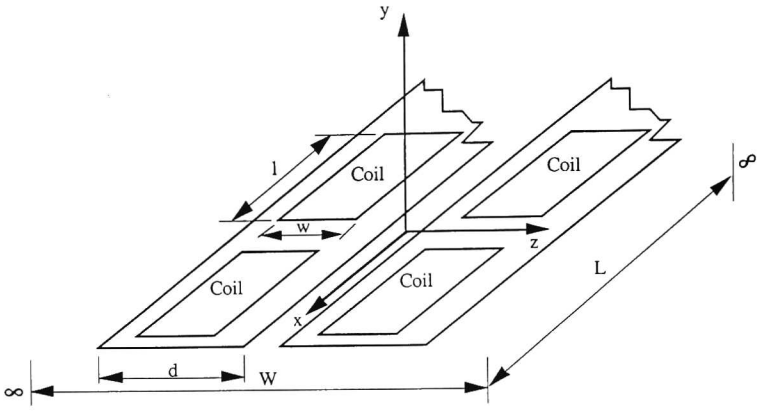

FIGURE 16 Coordinate and Fourier Series Base for Model of Levitation Magnet and Guideway System

The advantages of the approach are:

- It considers the finite width (d) of the guideway and can be used to analyze the transverse edge effects for the sheet guideway.
- It requires much less computational time and computer memory than the finite-element method.
- It is relatively simple to implement.

The shortcomings are:

- It considers only infinitely thin sheets.
- It is hard to transfer Cartesian coordinates to cylindrical coordinates, making it difficult to analyze the Magneplane system.

6.1.2 T-Method

There are many numerical approaches to solving 3-D eddy-current problems. Typical methods are the A-Φ method and the T-Ω method. Both methods require space variables and conductor variables, and, therefore, cannot deal effectively with open-boundary problems. In recent years, investigators have turned to another approach, called the T-method, in which the magnetic scalar potential Ω of the T-Ω method is not included (Takahashi and Kurita 1988; Toshiyuki et al. 1990; Tsuchimoto et al. 1992).

The advantages of the T-method are:

- Only one variable, T, is needed.
- There are no variables in space.
- It is easy to treat the external current and the external field.
- It can be used to analyze transverse edge effects for a flat-sheet guideway.

The disadvantages of the T-method are:

- The matrix, which contains nodes and other information, is dense compared with the finite-element method.
- The sheet is considered to be infinitely thin.
- The method cannot be transferred to cylindrical coordinates.

Some studies have applied the T-method to maglev research (Takahashi and Kurita 1988; Tsuchimoto et al. 1992). The following shows how the T-method applies to sheet-guideway problems.

The basic Maxwell equations are:

$$\nabla \times \tilde{H} = \tilde{J}\,, \qquad \nabla \times \tilde{E} = -\frac{\partial \tilde{B}}{\partial t}\,, \text{ and} \tag{1}$$

$$\tilde{B} = \mu_0 \tilde{H}\,, \qquad \tilde{J} = \sigma \tilde{E}\,, \tag{2}$$

where $\tilde{H}$, $\tilde{B}$, and $\tilde{J}$ are the magnetic-field, magnetic-induction, and current-density (the eddy-current density exists only in the plate) vectors; μ_0 is the magnetic permeability of air; and σ is the electrical conductivity. Since the eddy-current density is solenoidal and $\nabla \cdot \tilde{J} = 0$, the current vector potential, T, is defined as

$$\tilde{J} = \nabla \times \tilde{T} . \tag{3}$$

Note that T is not equal to H because T does not exist outside the conductor plate; H, however, does. From Equations 1-3 one can obtain

$$\nabla \times \left(\frac{1}{\sigma} \nabla \times \tilde{T} \right) = - \frac{\partial \tilde{B}}{\partial t} . \tag{4}$$

Assuming the conductor plate is thin enough and that the eddy current is induced by the z-component of the field B, as shown in Figure 17, the current vector potential T has only a z-component:

$$\frac{\partial^2 T_z}{\partial x^2} + \frac{\partial^2 T_z}{\partial y^2} = \sigma \frac{\partial B_z}{\partial t} . \tag{5}$$

T_z is assumed to be uniform through the thickness of the plate.

In the region of the conductor plate, Equation 5 can be discretized into the mesh distribution with any method, such as the finite-difference method. A matrix representation is expressed as follows:

$$[A]\{T_z\} = [A']\frac{\partial \{B_z\}}{\partial t} , \tag{6}$$

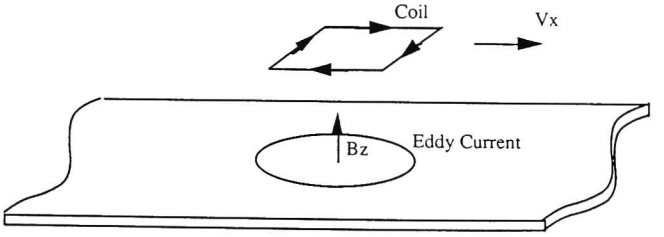

FIGURE 17 Repulsive Maglev Vehicle with a Coil

where [A] and [A'] are coefficient matrices. $\{B_z\}$ can be separated into two parts, B_t and B_e. B_t is the magnetic field produced from source coils on a vehicle; B_e is the reaction field from eddy currents in a plate. Equation 6 becomes

$$[A]\{T_z\} = [A']\frac{\partial\{B_t\}}{\partial t} + [A']\frac{\partial\{B_e\}}{\partial t} . \tag{7}$$

Assuming the source coils move along the x direction with constant velocity v_x, the first term of the right-hand side of Equation 7 becomes

$$[A']\frac{\partial\{B_t\}}{\partial t} = [A']\frac{\partial\{B_t\}}{\partial x}\frac{dx}{dt} = v_x[A']\frac{\partial\{B_t\}}{\partial x} . \tag{8}$$

B_t for each point on the plate can be obtained by Biot-Savart's equation. The reaction field B_e also can be obtained by Biot-Savart's equation, written in a matrix form:

$$\{B_e\} = [D_e]\{J_e\} , \tag{9}$$

where $[D_e]$ is a transformation matrix. From Equation 3, one can obtain the following relationship between J_e and T_z in the form of a matrix:

$$\{J_e\} = [C_e]\{T_z\} , \tag{10}$$

where $[C_e]$ is a transformation matrix.

Substituting Equations 8–10 into Equation 7, one obtains

$$[A]\{T_z\} = v_x[A']\frac{\partial\{B_t\}}{\partial t} + [A'][D_e][C_e]\frac{\partial\{T_z\}}{\partial t} . \tag{11}$$

This first-order differential equation in T_z can be numerically solved by a Runge-Kutta method and used to analyze the transient state of maglev systems. After T_z is solved, the eddy-current density J_e can be obtained by Equation 10, and the forces can be computed using the Lorenz Force Law.

6.1.3 EDDYCUFF Computer Code

EDDYCUFF is a 3-D eddy-current computer code developed by Mitsubishi Atomic Power Industries, Inc., and used by the MIT Plasma Fusion Center to analyze the Magneplane system. It solves integral equations using a finite-element method. The primary assumptions are that there is no current flow in the direction perpendicular to the sheet midplane and that the conducting medium

has a thickness that is small relative to its skin depth, i.e., the current density through the thickness is uniform. In practice, the thickness of the sheet guideway is ignored. The method is similar to the T-method except that the magnetic-vector potential A is used instead of the electrical potential T. EDDYCUFF software is currently available for the Sun Sparc and IBM RS6000 computers. The documents and manuals are not yet available in English.

6.1.4 Finite-Element Method with Upwinding

In principle, a 3-D finite-element method, such as ELEKTRA, can solve eddy-current problems for sheet guideways. However, there is a strict criterion that makes it difficult to practically analyze full-scale maglev systems at high speeds. The reason is that when the Peclet number is greater than 1, the solution oscillates and the result is very poor. This has long been a familiar problem in fluid dynamics. The solution is known as *upwinding* (Rodger et al. 1989). Vector Fields, Ltd., has used the upwinding technique to modify its ELEKTRA computer code. This new high-velocity code has been released but has not yet been tested.

6.2 New Computer Code Based on the Double-Fourier Series Method

As mentioned earlier, a double-Fourier series approach was used to analyze sheet-guideway problems (Ooi and Eastham 1975; Ooi 1979). The main advantage of the approach is that it can be used to analyze transverse edge effects for sheet guideways. The shortcoming is that the sheet is considered to be infinitely thin, meaning that the field is uniform through the thickness of the sheet. This assumption may cause large errors if the sheet is relatively thick. To overcome this disadvantage, Ooi's approach was studied in depth and a program was coded that duplicated his results. His theory was then extended by considering two or more layers to simulate the effect of the thickness in the sheet. Forces from our new ANL computer code were compared with ELEKTRA and with experimental data. The results are promising.

6.2.1 Programming Ooi's Method (Double-Fourier Series Method)

During coding of Ooi and Eastham's method, many problems were encountered. One problem was that his published papers were too brief and information was omitted or skipped over. Step-by-step re-derivation, therefore, was required. In addition, some typing errors and other problems had to be resolved. The errors in the papers are given in Appendix B.

An example taken from Ooi and Eastham was used for comparison of their results with results obtained from the program coded at ANL, as follows:

Magnet dimensions are:

Length	$l = 150$ cm
Width	$w = 30$ cm
Ampere-turns	$NI = 5 \times 10^5$ A-T
Suspension height	$h = 30$ cm

Guideway characteristics are:

Aluminum conductivity	$\sigma = 3.72 \times 10^7$ mho/m
Effective thickness	$t = 0.5$ cm

The magnet is designed to produce a lift of approximately four metric tons at a suspension height of 30 cm above the guideway surface at a cruising velocity of about 500 km/h. Figure 18 shows lift and drag forces vs. velocity curves for different strip guideway widths (d) from Ooi's model; Figure 19 shows the results from the new code. Figures 20 and 21 show the analogous effect of varying the suspension height (h). The lift and drag forces are plotted against strip guideway widths for a magnet width (w) of 0.3 m and a velocity (v) of 150 m/s. The new code closely duplicates results from Ooi's model.

In the example from Ooi and Eastham, the magnet was positioned in the center of the guideway. Ooi modified the formulation to calculate the transverse (or lateral) edge force for an off-center condition (Ooi 1975), as shown in Figure 22; results of the off-center condition are shown in Figure 23. The same forces were calculated using the new code with similar results, as shown in Figure 24. The only significant difference is that the guidance force decreases more rapidly in the new model than in Ooi's model when z_0 is greater than 0.2 m.

6.2.2 Extending Ooi's Method

In order to check the importance of the thickness of the sheet, we compared the results of Ooi's method with MAGFORCE results (assuming the sheet to be infinitely wide), as shown in Figure 25. (Note: the magnet and plate sizes are the same as in the example given by Ooi [Ooi

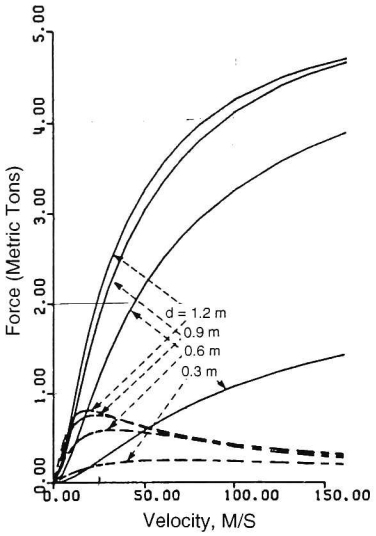

FIGURE 18 Lift (solid lines) and Drag (broken lines) Forces vs. Velocity for Various Strip Guideway Widths (d) — Ooi's Code (Source: Ooi and Eastham 1975)

1975].) The discrepancy between the two results is about 4–5%. Using Ooi's method with a 50.8- × 25.4- × 6.35-mm magnet moving over a 6.35-mm thick aluminum plate with a 12.7-mm suspension height, however, large differences occurred, as shown in Figure 26. In one case it was assumed that the equivalent eddy-current sheet was on the surface of the plate; in the second case the eddy-current sheet was assumed to be in the middle of the plate. The results produced using Ooi's code were either larger (30%) or smaller (20%) than the MAGFORCE results. The reason is that in Ooi's method the field through the thickness of the sheet is assumed to be uniform. When the sheet is thin enough (relative to the magnet size and air gap), this assumption is acceptable; when the sheet is relatively thick, however, this leads to a large error.

To overcome this shortcoming, Ooi's theory was extended by adding more layers to simulate a thick sheet. The eddy currents in those layers are not independent. After solving Maxwell's equations with the appropriate boundary conditions, expressions for eddy currents in each layer are obtained, and the Lorentz force $J \times B$ can be calculated to obtain the lift, drag, and guidance forces. The detailed derivations are given in Appendix A.

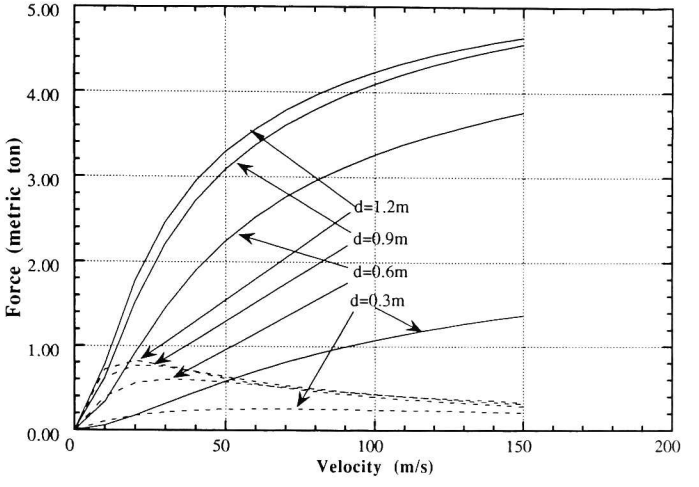

FIGURE 19 Lift and Drag Forces vs. Velocity for Various Strip Guideway Widths (d) — New Code

Figure 27 shows the force comparison for a 1.5- × 0.3-m coil suspended 0.3 m over a moving 5-mm-thick aluminum plate. Since the plate is thin, there is no large difference between the results obtained by modeling the sheet with one layer or five layers. Figures 28 and 29 show that the number of layers assumed makes a significant difference for a small magnet suspended close to a thick, moving sheet.

As described earlier, ELEKTRA simulated the edge effect for a small laboratory model quite well. However, it is very time-consuming; 3–4 h are required to obtain each point with reasonable accuracy. The double-Fourier series approach was used to calculate the force on a small rectangular coil (magnet) placed near the edge of a moving aluminum plate with results that compare well to ELEKTRA and to experimental data. Figure 30 shows the configuration of the experimental/computer-simulation model used. Three different H*s were simulated: H* = 12.7 mm (more than 100% overlap), H* = 0 (100% overlap), and H* = -12.7 mm (50% overlap), as shown in Figures 31 through 33.

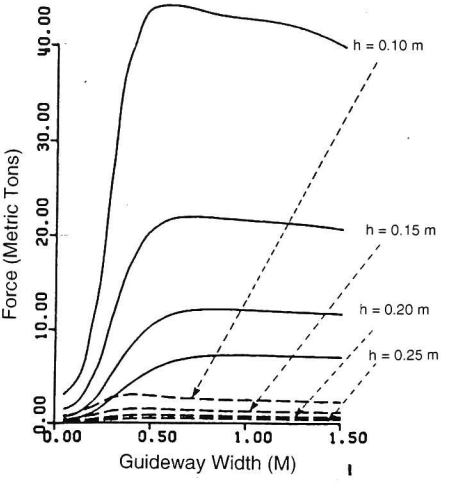

FIGURE 20 Lift (solid lines) and Drag (broken lines) Forces vs. Guideway Widths for Different Suspension Heights — Ooi's Code (magnet width = 0.3 m, velocity = 150 m/s) (Source: Ooi and Eastham 1975)

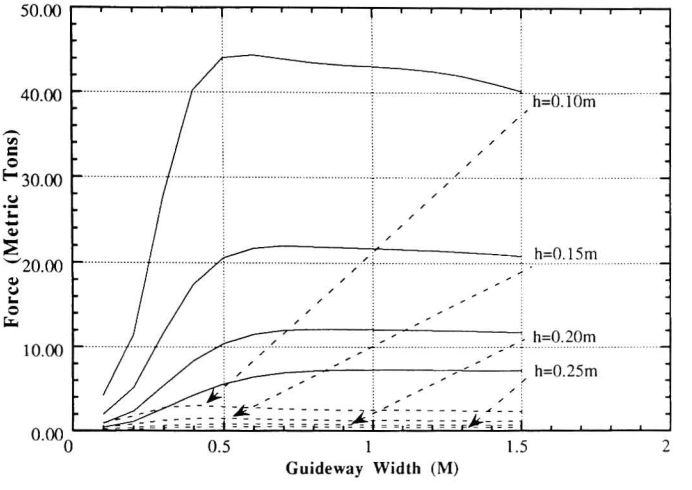

FIGURE 21 Lift and Drag Forces vs. Guideway Width for Different Suspension Heights — New Code (magnet width = 0.3 m, velocity = 150 m/s)

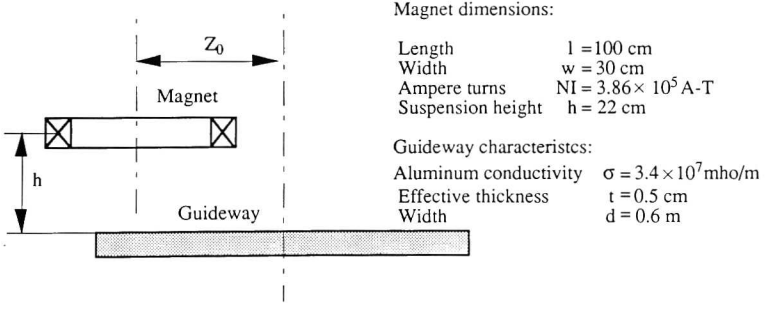

FIGURE 22 Simulated Model: Levitation Magnet at Transverse or Lateral Displacement z_0 from Guideway Centerline

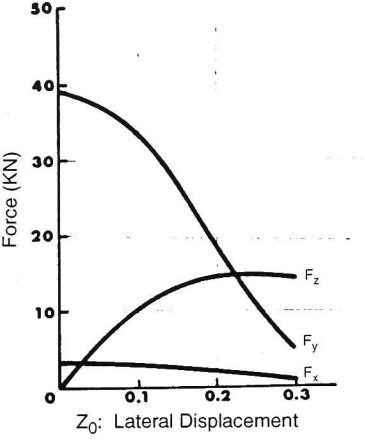

FIGURE 23 Forces vs. z_0 Characteristics for Figure 22 Simulated Model at 150 m/s — Ooi's Code (Source: Ooi 1975)

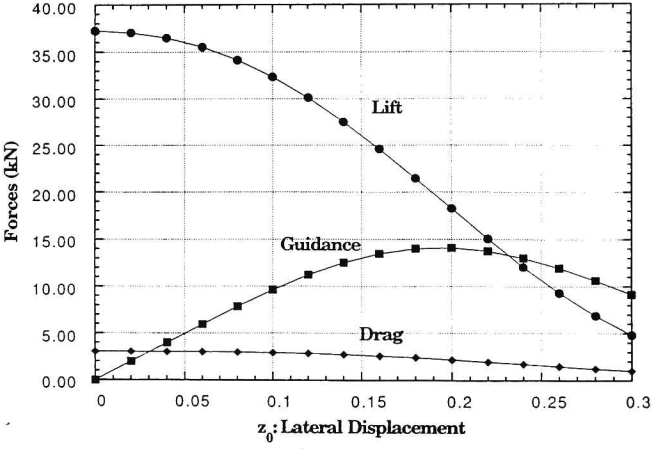

FIGURE 24 Forces vs. z_0 Characteristics for Figure 22 Simulated Model at 150 m/s — New Code

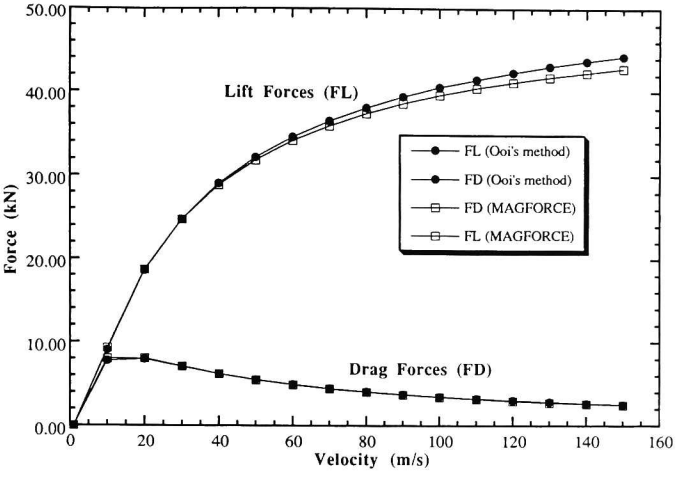

FIGURE 25 A 1.5- × 0.3-m Coil Suspended 0.3 m over a Moving 5-mm-Thick Aluminum Plate; NI = 5 × 10^5 A-T

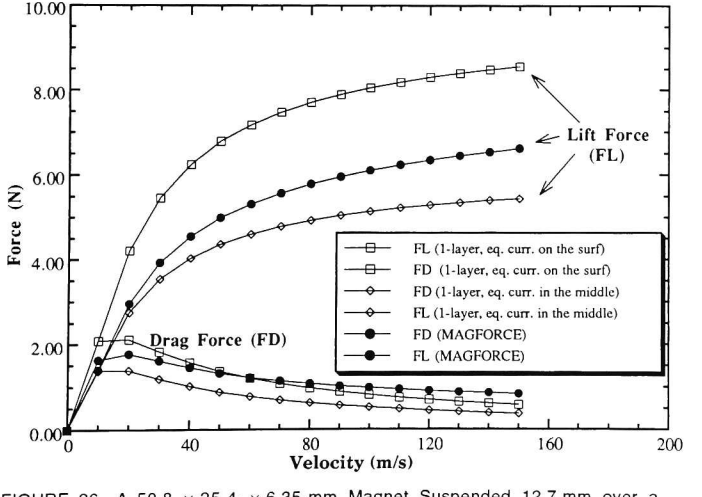

FIGURE 26 A 50.8- × 25.4- × 6.35-mm Magnet Suspended 12.7 mm over a Moving 6.35-mm-Thick Aluminum Plate; NI = 5,994 A-T

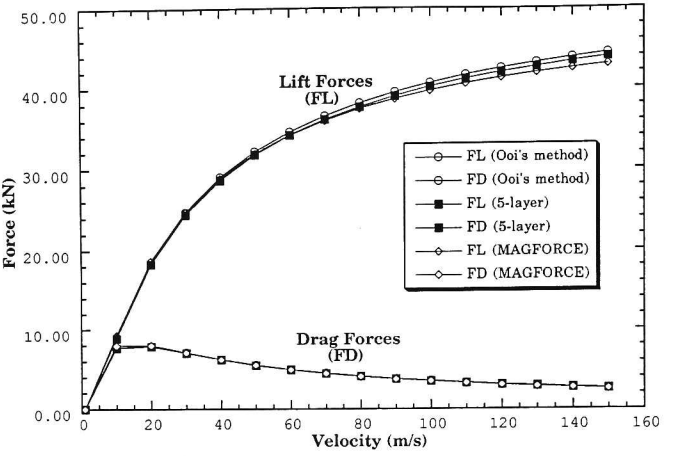

FIGURE 27 Calculated Lift and Drag Forces for a 1.5- × 0.3-m Coil Suspended 0.3 m over a Moving 5-mm-Thick Aluminum Plate; NI = 5×10^5 A-T

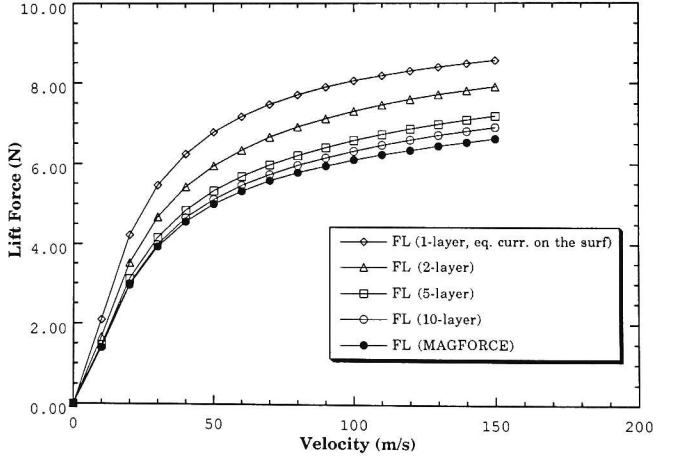

FIGURE 28 Lift Force for a 50.8- × 25.4- × 6.35-mm Magnet Suspended 12.7 mm over a Moving 6.35-mm-Thick Aluminum Plate; NI = 5,994 A-T

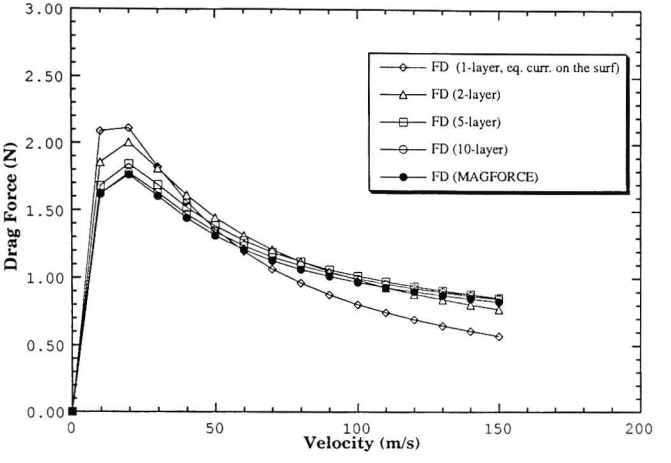

FIGURE 29 Drag Force for a 50.8- × 25.4- × 6.35-mm Magnet Suspended 12.7 mm over a Moving 6.35-mm-Thick Aluminum Plate; NI = 5,994 A-T

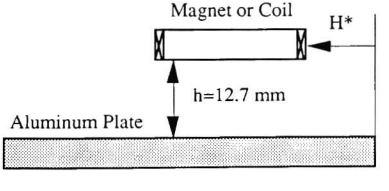

Magnet or coil dimensions:

Length	l = 50.8 mm
Width	w = 25.4 mm
Thickness	t = 6.35 mm
Ampere turns	NI = 5715 A-T
Suspension height	h = 12.7 mm

Guideway characteristcs:

Aluminum conductivity	$\sigma = 2.5 \times 10^7$ mho/m
Thickness	t = 6.35 mm
Width	d = 101 mm

FIGURE 30 Configuration of the Experimental/Computer-Simulation Model

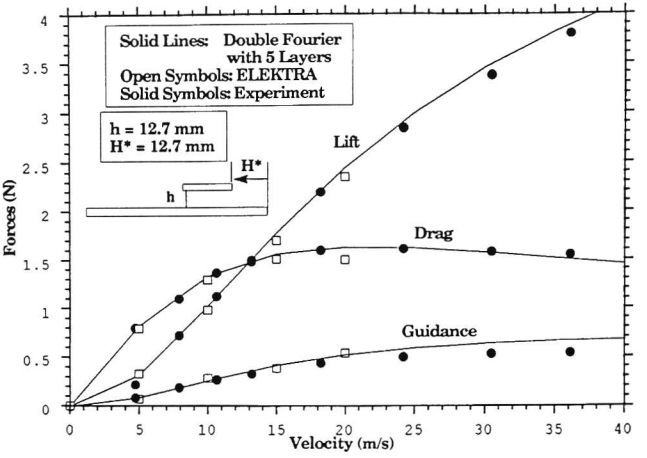

FIGURE 31 Force on a 50.8- × 25.4- × 6.35-mm Magnet Suspended over a Moving 6.35-mm-Thick Aluminum Plate; H* = 12.7 mm

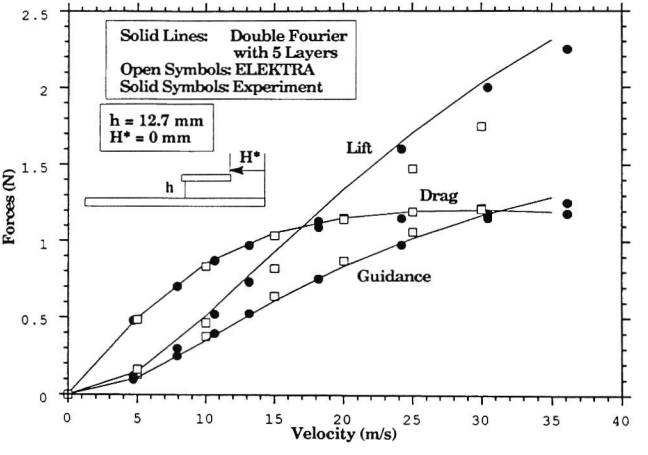

FIGURE 32 Force on a 50.8- × 25.4- × 6.35-mm Magnet Suspended over a Moving 6.35-mm-Thick Aluminum Plate; H* = 0 mm

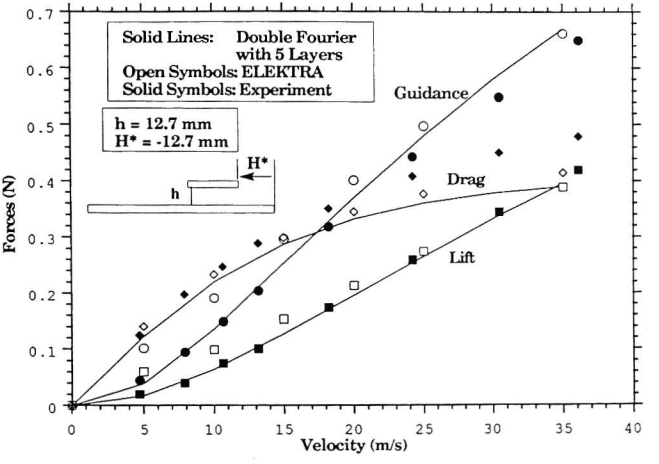

FIGURE 33 Force on a 50.8- × 25.4- × 6.35-mm Magnet Suspended over a Moving 6.35-mm-Thick Aluminum Plate; H* = -12.7 mm

7 Conclusions

The existing ELEKTRA computer code is capable of performing basic calculations for three-dimensional, small-scale models of maglev with a continuous-sheet guideway. The ELEKTRA results matched the experimental data and the MAGFORCE results quite well at intermediate velocities. When using this code at very low speeds (less than 5 m/s), users should be very careful because numerical errors may occur. In order to avoid numerical errors, finer mesh distributions have to be designed and nonstandard force commands have to be used in the post-processor. To date, because of numerical instability, ELEKTRA cannot simulate large-scale, full-velocity maglev systems while using the Sun Sparc computer system. The new ANL double-Fourier series computer program has proved to be a useful tool for analyzing continuous-sheet guideway maglev problems, including transverse (lateral) edge effects. By adding more layers of current sheets, to simulate the thickness of the sheet, the accuracy of the results is greatly increased, especially when the sheet is thick. The force calculations are in close agreement with the experimental data.

Vector Fields, Ltd., recently released a new high-velocity version of ELEKTRA in which the upwinding technique was used. The new version is supposed to be capable of simulating high-velocity, full-scale maglev systems. Additional research will be required to test and validate the new velocity version.

8 References

Coffey, H.C., J. He, and Z. Wang, 1993, "Corroboration of Magnetic Forces in U.S. Maglev Design," presented at the 13th International Conference on Magnetically Levitated Systems and Linear Drives, May 19-21, Argonne National Laboratory, Argonne, Ill., pp. 304-309.

Coffey, H.T., F. Chilton, and L.O. Hoppie, 1972, "The Feasibility of Magnetically Levitating High Speed Ground Vehicle," National Technical Information Service Publication 210505, Feb., based on Frank Chilton and Howard Coffey, "Magnetic Levitation: Tomorrow's Transportation," May 1971, The Helium Society, Washington, D.C., and J.R. Reitz and L.C. Davis, "Force on a Rectangular Coil Moving above a Conducting Slab," *Journal Applied Physics*, vol. 43, no. 4, April 1972.

Hull, J.R., 1992, unpublished information, Argonne National Laboratory, Argonne, Ill.

Ooi, B.T., 1975, "Transverse Force in Magnetic Levitation with Finite-Width Sheet Guideways," Institute of Electrical and Electronic Engineers, *IEEE Transactions on Power Apparatus and Systems,* vol. PAS-94, no. 3, May/June, pp. 994-1002.

Ooi, B.T., and A.R. Eastham, 1975, "Transverse Edge Effects of Sheet Guideways in Magnetic Levitation," Institute of Electrical and Electronic Engineers, *IEEE Transactions on Power Apparatus and Systems*, vol. PAS-94, no. 1, Jan./Feb., pp. 82-80.

Rodger, D., et al. , 1989, "A Formulation for 3-D Moving Conductor Eddy Current Problems," Institute of Electrical and Electronic Engineers, *IEEE Transactions on Magnetics*, 25(5):4147-4149, Sept.

Takahashi, T., and K. Kurita, 1988, "Computation of Eddy Currents Induced in a Conducting Sheet under Moving Magnets," Institute of Electrical and Electronic Engineers, *IEEE Transactions on Magnetics*, 24(1):197-200, Jan.

Toshiyuki, T., et al., 1990, "Experimental Verification of 3-D Eddy Current Analysis Code Using T-Method," Institute of Electrical and Electronic Engineers, *IEEE Transactions on Magnetics,* 26(2):474-477, March.

Tsuchimoto, M., et al., 1992, "An Analysis of Eddy Current and Lorentz Force of Thin Plates under Moving Magnets," Institute of Electrical and Electronic Engineers, *IEEE Transactions on Magnetics,* 28(2):1434-1437, March.

Appendix A:

Summation and Expansion of the Double-Fourier Series Method

Appendix A:

Summation and Expansion of the Double-Fourier Series Method

The major difference between our approach and Ooi's method is the expression for the magnetic field intensity. Other parts are almost the same, except that we represent the guideway as multilayer eddy-current sheets.

The summation and expansion of the double-Fourier series method consists of four parts.

1. *Magnetic Field Intensity*

We found the magnetic field intensity $\tilde{H}$ at different layers of the guideway (Figure A.1). The y-component of H was used in the guideway interaction, and the x- and z-components were used to calculate forces. In this part, only the finite thickness is considered; finite-width effects are considered later. A general expression for the three components of $\tilde{H}$ in a double-Fourier series is

$$(H_{ik})_{y=y_k} = \mathrm{Real}\sum_{n=1}^{N}\sum_{m=1}^{M} \begin{matrix} D_i\left(A_{Smn}\, e^{\beta|h_S-h_k|} + \sum_{j=1}^{NL} A_{Rjmn}\, e^{\beta|h_j-h_k|} \right) e^{j(\alpha x+\gamma z)} \\ + D_i\left(B_{Smn}\, e^{\beta|h_S-h_k|} + \sum_{i=1}^{NL} B_{Rjmn}\, e^{\beta|h_j-h_k|} \right) e^{j(\alpha x-\gamma z)} \end{matrix} \quad (i=x,y,z),\ (k=1,2,\ldots NL)\ , (A.1)$$

where D_i is a coefficient containing constants and other parameters; A_{Smn} and B_{Smn} are the Fourier coefficients of the source coil, which are known; A_{Rjmn} and B_{Rjmn} are the Fourier coefficients of the guideway of the jth layer, which are unknown and to be solved.

2. *Guideway Modeling*

A coefficient C_{lm} is used to consider the effect of the finite width of the guideway. We will find the relationship between A_{Rjmn}, B_{Rjmn}, and C_{lm}.

3. *Guideway Interactions*

Maxwell's equations and power equality equation will be used to obtain C_{lm} in the matrix forms.

4. *Electromechanical Forces*

The Lorentz force will be applied to all the layers of the guideway to calculate total lift, drag, and guidance forces.

A.1 Magnetic Field Intensity

For clarity, consider a three-current sheet guideway, as shown in Figure A.1. The derivation is similar if additional sheets are added. In the following derivations, subscript "S" denotes the stator (superconductor coils) and subscript "R" denotes the rotor (the conductor plate).

In the model, all space is divided into five regions, regions I to V. The superconducting magnet is represented by four rectangular filaments, each of which can be regarded as a sheet current $\tilde{K}_S$ in the plane y = h. $\tilde{K}_S$ can be written in the following form:

$$\begin{aligned}\tilde{K}_S &= \sum_{n=1,3,5\ldots}^{N} \sum_{m=1,3,5,\ldots}^{M} \left(2\gamma A_{Smn} \cos(\gamma z) \sin(\alpha x)\vec{i} - 2\alpha A_{Smn} \sin(\gamma z) \cos(\alpha x)\vec{k}\right) \\ &= \sum_{n=1,3,5\ldots}^{N} \sum_{m=1,3,5,\ldots}^{M} \left(K_{Sxr} \cos(\gamma z) \sin(\alpha x)\vec{i} - K_{Szr} \sin(\gamma z) \cos(\alpha x)\vec{k}\right),\end{aligned} \tag{A.2}$$

where $K_{Sxr} = 2\gamma A_{Smn}$, $K_{Szr} = 2\alpha A_{Smn}$, $\alpha = 2\pi m/L$, and $\gamma = 2\pi n/W$; L is the Fourier period in the x-direction (motion direction), and W is the Fourier period in the z-direction, transverse (lateral) direction, as shown in Figure 16.

Equation A.2 can also be written in the following equivalent form:

$$\tilde{K}_S = \nabla \times \tilde{U}_y \sum_{n=1,3,5\ldots}^{N} \sum_{m=1,3,5,\ldots}^{M} (2A_{Smn} \sin(\gamma z) \sin(\alpha x)), \tag{A.3}$$

where $\tilde{U}_y$ is a unit vector. Since the magnet is represented by the four rectangular filaments which produce the space impulses, the shape of the derivative of the space impulses is as shown in Figure A.2.

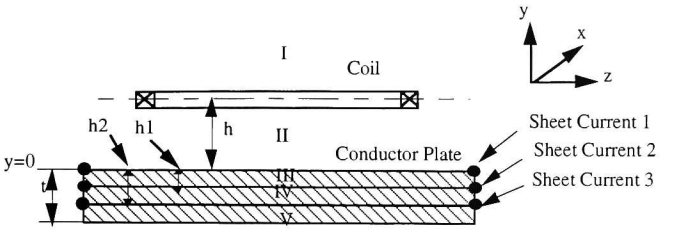

FIGURE A.1 Model of Multiple Layers of Sheet Currents to Simulate the Conductor Plate

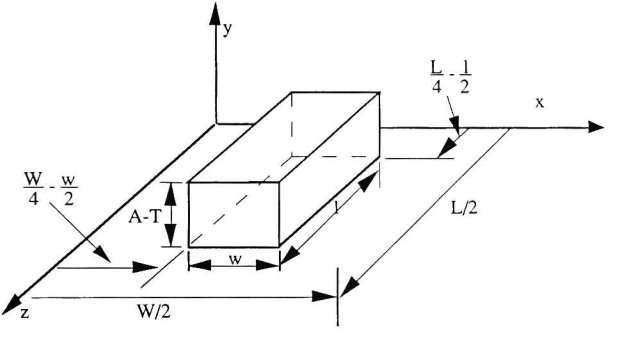

FIGURE A.2 Model for Determining the Double-Fourier Coefficients A_{Smn}

A_{Smn} can be determined by the following formula:

$$A_{Smn} = \frac{8\ A\text{-}T}{WL} \int_0^{\frac{L}{2}} \int_0^{\frac{W}{2}} \sin(\alpha x)\, \sin(\gamma z)\, dx\, dz$$

$$= \frac{8\ A\text{-}T}{\alpha\, \gamma\, WL} \left(\cos \gamma\left(\frac{W}{4} - \frac{w}{2}\right) - \cos \gamma\left(\frac{W}{4} + \frac{w}{2}\right)\right)\left(\cos \alpha\left(\frac{L}{4} - \frac{1}{2}\right) - \cos \alpha\left(\frac{L}{4} + \frac{1}{2}\right)\right)$$

$$= \frac{A\text{-}T}{nm} \frac{8}{\pi^2} \sin\left(\frac{n\pi}{2}\right) \sin\left(\frac{m\pi}{2}\right) \sin\left(\frac{n\pi w}{W}\right) \sin\left(\frac{n\pi l}{L}\right), \qquad (A.4)$$

where A-T is the ampere turns of the magnet. Note that $\widetilde{K}_S$ must be selected to satisfy $\nabla \widetilde{K}_S = 0$. Equation A.2 can also be written in the complex form (Ooi and Eastham 1975):

$$\widetilde{K}_S = \text{Real}\ \nabla \times \widetilde{U}_y \sum_{n=1,3,5\ldots}^{N} \sum_{m=1,3,5,\ldots}^{M} \left(A_{Smn}\, e^{j(\alpha x + \gamma z)} + B_{Smn}\, e^{j(\alpha x - \gamma z)}\right), \qquad (A.5)$$

where $B_{Smn} = -A_{Smn}$.

For the example in Figure A.1, the guideway plate is composed of three sheet currents $\widetilde{K}_{R1}$, $\widetilde{K}_{R2}$, and $\widetilde{K}_{R3}$. $\widetilde{K}_{Rk}$ (k = 1,2,3) can be written in the form of double-Fourier series.

$$K_{Rk} = \sum_{n=1,3,5\ldots}^{N} \sum_{m=1,3,5,\ldots}^{M} \left(2\gamma A_{Rkmn} \cos(\gamma z)\, \sin(\alpha x + \phi_k)\vec{i} - 2\alpha A_{Rkmn} \sin(\gamma z)\, \cos(\alpha x + \phi_k)\vec{k}\right),$$

$$(k = 1,2,3). \qquad (A.6)$$

Note that the difference between $\widetilde{K}_S$ and $\widetilde{K}_{Rk}$ (k = 1,2,3) is that $\widetilde{K}_{Rk}$ has a delay angle ϕ_k. A_{Rkmn} is unknown and is to be solved. $\widetilde{K}_{Rk}$ (k = 1,2,3) can also be written in the following form:

$$K_{Rk} = \sum_{n=1,3,5\ldots}^{N} \sum_{m=1,3,5,\ldots}^{M} 2\gamma(A_{Rkrmn}\cos(\gamma z)\sin(\alpha x) + A_{Rkimn}\cos(\gamma z)\cos(\alpha x))\vec{i} - 2\alpha(A_{Rkrmn}\sin(\gamma z)\cos(\alpha x) + A_{Rkimn}\sin(\gamma z)\sin(\alpha x))\vec{k}$$

$$= \sum_{n=1,3,5\ldots}^{N} \sum_{m=1,3,5,\ldots}^{M} (K_{Rkxr}\cos(\gamma z)\sin(\alpha x) + K_{Rkxi}\cos(\gamma z)\cos(\alpha x))\vec{i} - (K_{Rkzr}\sin(\gamma z)\cos(\alpha x) + K_{Rkzi}\sin(\gamma z)\sin(\alpha x))\vec{k}, \quad k = 1,2,3, \quad (A.7)$$

where $A_{Rkrmn} = A_{Rkmn}\cos\phi_k$, $A_{Rkimn} = A_{Rkmn}\sin\phi_k$, $K_{Rkxr} = 2\gamma A_{Rkrmn}$, $K_{Rkxi} = 2\gamma A_{Rkimn}$, $K_{Rkzr} = 2\alpha A_{Rkrmn}$, and $K_{Rkzi} = 2\alpha A_{Rkjimn}$.

Using the vector potential $\widetilde{A}$ as a variable, we solve the Maxwell's equations:

$$\frac{\partial A_x^2}{\partial x^2} + \frac{\partial A_x^2}{\partial y^2} + \frac{\partial A_x^2}{\partial z^2} = 0 \quad (A.8)$$

and

$$\frac{\partial A_z^2}{\partial x^2} + \frac{\partial A_z^2}{\partial y^2} + \frac{\partial A_z^2}{\partial z^2} = 0\ . \quad (A.9)$$

Since the current in the coil is assumed to be represented by a double-Fourier series in a harmonic form, the solution of Maxwell equations should also be of this form to satisfy the boundary conditions. The boundary conditions are that the fields must vanish at $y = \pm\infty$, and

$$H_{1x} - H_{2x} = -K_z \quad \text{and} \quad H_{1z} - H_{2z} = K_x$$

or

$$\frac{1}{\mu_0}\left(\frac{\partial A_{1z}}{\partial y} - \frac{\partial A_{2z}}{\partial y}\right) = -K_z \quad \text{and} \quad \frac{1}{\mu_0}\left(\frac{\partial A_{1x}}{\partial y} - \frac{\partial A_{2x}}{\partial y}\right) = K_x\ , \quad (A.10)$$

where subscripts 1 and 2 denote the field immediately on either side of the discontinuity. Therefore, the solution of one of the harmonic solutions (nth in transverse [lateral] direction [z] and mth in motion direction [x]) for five regions are:

$$A_{Ix} = E_1 e^{-\beta y}\sin(\alpha x)\cos(\gamma z) + E_5 e^{-\beta y}\cos(\alpha x)\cos(\gamma z)\ ,$$

$$A_{Iz} = E_3 e^{-\beta y}\cos(\alpha x)\sin(\gamma z) + E_7 e^{-\beta y}\sin(\alpha x)\sin(\gamma z)\ ,$$

$$A_{IIx} = (D_1 e^{-\beta y} + D_2 e^{\beta y}) \sin(\alpha x) \cos(\gamma z) + (D_5 e^{-\beta y} + D_6 e^{\beta y}) \cos(\alpha x) \cos(\gamma z) ,$$

$$A_{IIz} = (D_3 e^{-\beta y} + D_4 e^{\beta y}) \cos(\alpha x) \sin(\gamma z) + (D_7 e^{-\beta y} + D_8 e^{\beta y}) \sin(\alpha x) \sin(\gamma z) ,$$

$$A_{IIIx} = (G_1 e^{-\beta y} + G_2 e^{\beta y}) \sin(\alpha x) \cos(\gamma z) + (G_5 e^{-\beta y} + G_6 e^{\beta y}) \cos(\alpha x) \cos(\gamma z) ,$$

$$A_{IIIz} = (G_3 e^{-\beta y} + G_4 e^{\beta y}) \cos(\alpha x) \sin(\gamma z) + (G_7 e^{-\beta y} + G_8 e^{\beta y}) \sin(\alpha x) \sin(\gamma z) ,$$

$$A_{IVx} = (C_1 e^{-\beta y} + C_2 e^{\beta y}) \sin(\alpha x) \cos(\gamma z) + (C_5 e^{-\beta y} + C_6 e^{\beta y}) \cos(\alpha x) \cos(\gamma z) ,$$

$$A_{IVz} = (C_3 e^{-\beta y} + C_4 e^{\beta y}) \cos(\alpha x) \sin(\gamma z) + (C_7 e^{-\beta y} + C_8 e^{\beta y}) \sin(\alpha x) \sin(\gamma z) ,$$

$$A_{Vx} = S_2 e^{\beta y} \sin(\alpha x) \cos(\gamma z) + S_6 e^{\beta y} \cos(\alpha x) \cos(\gamma z) ,$$

and

$$A_{Vz} = S_4 e^{\beta y} \cos(\alpha x) \sin(\gamma z) + S_8 e^{\beta y} \sin(\alpha x) \sin(\gamma z) ,$$

where $\beta = \sqrt{\alpha^2 + \gamma^2}$. (A.11)

Then the boundary conditions are used to determine the coefficients E_1, E_3, E_5, E_7, D_1, D_2, D_3, D_4, D_5, D_6, D_7, D_8, G_1, G_2, G_3, G_4, G_5 G_6, G_7, G_8, C_1, C_2, C_3, C_4, C_5, C_6, C_7, C_8, S_2, S_4, S_6, and S_8.

The relationship between $\tilde{H}$ and $\tilde{A}$ is

$$\tilde{H} = \frac{1}{\mu_0} \nabla \times \tilde{A} = \frac{1}{\mu_0} \left(\frac{\partial A_z}{\partial y} \vec{i} + \left(\frac{\partial A_x}{\partial z} - \frac{\partial A_z}{\partial x} \right) \vec{j} - \frac{\partial A_x}{\partial y} \vec{k} \right) . \quad (A.12)$$

At y = h, the boundary conditions are:

$$H_{Ix} - H_{IIx} = -K_{Sz}, \; H_{Iz} - H_{IIz} = K_{Sx}, \; A_{Ix} = A_{IIx} , \text{ and } A_{Iz} = A_{IIz} ,$$

where

$$H_{Ix} = \frac{1}{\mu_0} \frac{\partial A_{Iz}}{\partial y} = -\frac{1}{\mu_0} \beta \left(E_3 e^{-\beta y} \cos(\alpha x) \sin(\gamma z) + E_7 e^{-\beta y} \sin(\alpha x) \sin(\gamma z) \right) ,$$

$$H_{Iz} = \frac{1}{\mu_0} \frac{\partial A_{Ix}}{\partial y} = -\frac{1}{\mu} \beta \left(E_1 e^{-\beta y} \sin(\alpha x) \cos(\gamma z) + E_5 e^{-\beta y} \cos(\alpha x) \cos(\gamma z) \right) ,$$

$$H_{IIx} = \frac{1}{\mu_0}\frac{\partial A_{IIz}}{\partial y} = \frac{\beta}{\mu_0}\left(-D_3\, e^{-\beta y} + D_4\, e^{\beta y}\right)\cos(\alpha x)\,\sin(\gamma z)$$

$$+ \frac{\beta}{\mu_0}\left(-D_7\, e^{-\beta y} + D_8\, e^{\beta y}\right)\sin(\alpha x)\,\sin(\gamma z)\ ,$$

$$H_{IIz} = \frac{1}{\mu_0}\frac{\partial A_{IIx}}{\partial y} = \frac{\beta}{\mu_0}\left(-D_1\, e^{-\beta y} + D_2\, e^{\beta y}\right)\sin(\alpha x)\,\cos(\gamma z)$$

$$+ \frac{\beta}{\mu_0}\left(-D_5\, e^{-\beta y} + D_6\, e^{\beta y}\right)\cos(\alpha x)\,\cos(\gamma z)\ ,$$

$$K_{Sx} = K_{Sxr}\cos(\gamma z)\,\sin(\alpha x), \quad \text{and} \quad K_{Sz} = K_{Szr}\sin(\gamma z)\,\cos(\alpha x)\ . \tag{A.13}$$

Therefore,

$$\beta\left(-E_1 e^{-\beta h} + D_1 e^{-\beta h} - D_2 e^{\beta h}\right) = \mu_0 K_{Sxr}\ , \qquad \left(-E_5 e^{-\beta h} + D_5 e^{-\beta h} - D_6 e^{\beta h}\right) = 0\ ,$$

$$\beta\left(-E_3 e^{-\beta h} + D_3 e^{-\beta h} - D_4 e^{\beta h}\right) = -\mu_0 K_{Szr}\ , \qquad \left(-E_7 e^{-\beta h} + D_7 e^{-\beta h} - D_8 e^{\beta h}\right) = 0\ ,$$

$$\left(-E_1 e^{-\beta h} + D_1 e^{-\beta h} - D_2 e^{\beta h}\right) = 0\ , \qquad -E_5 e^{-\beta h} - D_5 e^{-\beta h} - D_6 e^{\beta h} = 0\ ,$$

$$-E_3 e^{-\beta h} - D_3 e^{-\beta h} - D_4 e^{\beta h} = 0\ , \quad \text{and} \quad -E_7 e^{-\beta h} - D_7 e^{-\beta h} - D_8 e^{\beta h} = 0\ . \tag{A.14}$$

Similarly, at $y = 0$:

$$\beta\,(-D_1 + D_2 + G_1 - G_2) = \mu_0 K_{R1xr}\ , \qquad \beta\,(-D_5 + D_6 + G_5 - G_6) = \mu_0 K_{R1xi}\ ,$$

$$\beta\,(-D_3 + D_4 + G_3 - G_4) = -\mu_0 K_{R1zr}\ , \qquad \beta\,(-D_7 + D_8 + G_7 - G_8) = -\mu_0 K_{R1zi}\ ,$$

$$D_1 + D_2 - G_1 - G_2 = 0\ , \qquad D_5 + D_6 - G_5 - G_6 = 0\ ,$$

$$D_3 + D_4 - G_3 - G_4 = 0\ , \quad \text{and} \quad D_7 + D_8 - G_7 - G_8 = 0\ .$$

At $y = h_1$:

$$\beta\left(-G_2e^{\beta h_1} + G_2e^{\beta h_1} + C_1e^{-\beta h_1} - C_2e^{\beta h_1}\right) = \mu_0 K_{R2xr}\,, \qquad \beta\left(-G_5e^{\beta h_1} + G_6e^{\beta h_1} + C_5e^{-\beta h_1} - C_6e^{\beta h_1}\right) = \mu_0 K_{R2xi}\,,$$

$$\beta\left(-G_3e^{\beta h_1} + G_4e^{\beta h_1} + C_3e^{-\beta h_1} - C_4e^{\beta h_1}\right) = -\mu_0 K_{R2zr}\,, \qquad \beta\left(-G_7e^{\beta h_1} + G_8e^{\beta h_1} + C_7e^{-\beta h_1} - C_8e^{\beta h_1}\right) = -\mu_0 K_{R2zi}\,,$$

$$G_1e^{-\beta h_1} + G_2e^{\beta h_1} - C_1e^{-\beta h_1} - C_2e^{\beta h_1} = 0, \qquad G_5e^{-\beta h_1} + G_6e^{\beta h_1} - C_5e^{-\beta h_1} - C_6e^{\beta h_1} = 0,$$

$$G_3e^{-\beta h_1} + G_4e^{\beta h_1} - C_3e^{-\beta h_1} - C_4e^{\beta h_1} = 0, \quad \text{and} \quad G_7e^{-\beta h_1} + G_8e^{\beta h_1} - C_7e^{-\beta h_1} - C_8e^{\beta h_1} = 0.$$

At $y = h_2$:

$$\beta\left(-C_1e^{-\beta h_2} + C_2e^{\beta h_2} - K_2e^{\beta h_2}\right) = \mu_0 K_{R3xr}, \qquad \beta\left(-C_5e^{-\beta h_2} + C_6e^{\beta h_2} - K_6e^{\beta h_2}\right) = \mu_0 K_{R3xi},$$

$$\beta\left(-C_3e^{-\beta h_2} + C_4e^{\beta h_2} - K_4e^{\beta h_2}\right) = -\mu_0 K_{R3zr}, \qquad \beta\left(-C_7e^{-\beta h_2} + C_8e^{\beta h_2} - K_8e^{\beta h_2}\right) = -\mu_0 K_{R3zi}\,,$$

$$C_1e^{-\beta h_2} + C_2e^{\beta h_2} - S_2e^{\beta h_2} = 0, \qquad C_5e^{-\beta h_2} + C_6e^{\beta h_2} - S_6e^{\beta h_2} = 0,$$

$$C_3e^{-\beta h_2} + C_4e^{\beta h_2} - S_4e^{\beta h_2} = 0, \quad \text{and} \quad C_7e^{-\beta h_2} + C_8e^{\beta h_2} - S_8e^{\beta h_2} = 0. \qquad \text{(A.15)}$$

Solving these 32 equations, we can obtain 32 coefficients:

$$E_1 = -\frac{\mu_0}{2\beta}\left(K_{Sxr}e^{\beta h} + K_{R1xr} + K_{R2xr}e^{\beta h_1} + K_{R3xr}e^{\beta h_2}\right), \qquad E_5 = -\frac{\mu_0}{2\beta}\left(K_{R1xi} + K_{R2xi}e^{\beta h_1} + K_{R3xi}e^{\beta h_2}\right),$$

$$E_3 = \frac{\mu_0}{2\beta}\left(K_{Szr}e^{\beta h} + K_{R1zr} + K_{R2zr}e^{\beta h_1} + K_{R3zr}e^{\beta h_2}\right), \qquad E_7 = \frac{\mu_0}{2\beta}\left(K_{R1zi} + K_{R2zi}e^{\beta h_1} + K_{R3zi}e^{\beta h_2}\right),$$

$$D_1 = -\frac{\mu_0}{2\beta}\left(K_{R1xr} + K_{R2xr}e^{\beta h_1} + K_{R3xr}e^{\beta h_2}\right), \qquad D_5 = -\frac{\mu_0}{2\beta}\left(K_{R1xi} + K_{R2xi}e^{\beta h_1} + K_{R3xi}e^{\beta h_2}\right),$$

$$D_2 = -\frac{\mu_0}{2\beta}K_{Sxr}e^{-\beta h}, \qquad D_6 = 0,$$

$$D_3 = \frac{\mu_0}{2\beta}\left(K_{R1zr} + K_{R2zr}e^{\beta h_1} + K_{R3zr}e^{\beta h_2}\right), \qquad D_7 = \frac{\mu_0}{2\beta}\left(K_{R1zi} + K_{R2zi}e^{\beta h_1} + K_{R3zi}e^{\beta h_2}\right),$$

$$D_4 = \frac{\mu_0}{2\beta} K_{Szr}e^{-\beta h}, \qquad D_8 = 0,$$

$$G_1 = -\frac{\mu_0}{2\beta}\left(K_{R2xr}e^{\beta h_1} + K_{R3xr}e^{\beta h_2}\right), \qquad G_5 = -\frac{\mu_0}{2\beta}\left(K_{R2xi}e^{\beta h_1} + K_{R3xi}e^{\beta h_2}\right),$$

$$G_2 = -\frac{\mu_0}{2\beta}\left(K_{Sxr}e^{-\beta h} + K_{R1xr}\right), \qquad G_6 = -\frac{\mu_0}{2\beta}\left(K_{R1xi}\right),$$

$$G_3 = \frac{\mu_0}{2\beta}\left(K_{R2zr}e^{\beta h_1} + K_{R3zr}e^{\beta h_2}\right), \qquad G_7 = \frac{\mu_0}{2\beta}\left(K_{R2zi}e^{\beta h_1} + K_{R3zi}e^{\beta h_2}\right),$$

$$G_4 = \frac{\mu_0}{2\beta}\left(K_{Szr}e^{-\beta h} + K_{R1zr}\right), \qquad G_8 = \frac{\mu_0}{2\beta}\left(K_{R1zi}\right),$$

$$C_1 = -\frac{\mu_0}{2\beta} K_{R3xr}e^{\beta h_2}, \qquad C_5 = -\frac{\mu_0}{2\beta} K_{R3xi}e^{\beta h_2},$$

$$C_2 = -\frac{\mu_0}{2\beta}\left(K_{Sxr}e^{-\beta h} + K_{R1xr} + K_{R2xr}e^{-\beta h_1}\right), \qquad C_6 = -\frac{\mu_0}{2\beta}\left(K_{R1xi} + K_{R2xi}e^{-\beta h_1}\right),$$

$$C_3 = \frac{\mu_0}{2\beta} K_{R3zr}e^{\beta h_2}, \qquad C_7 = \frac{\mu_0}{2\beta} K_{R3zi}e^{\beta h_2},$$

$$C_4 = \frac{\mu_0}{2\beta}\left(K_{Szr}e^{-\beta h} + K_{R1zr} + K_{R2zr}e^{-\beta h_1}\right), \qquad C_8 = \frac{\mu_0}{2\beta}\left(K_{R1zi} + K_{R2zi}e^{-\beta h_1}\right),$$

$$S_2 = -\frac{\mu_0}{2\beta}\left(K_{Sxr}e^{-\beta h} + K_{R1xr} + K_{R2xr}e^{-\beta h_1} + K_{R3xr}e^{-\beta h_2}\right), \quad S_6 = -\frac{\mu_0}{2\beta}\left(K_{R1xi} + K_{R2xi}e^{-\beta h_1} + K_{R3xi}e^{-\beta h_2}\right),$$

$$S_4 = \frac{\mu_0}{2\beta}\left(K_{Szr}e^{-\beta h} + K_{R1zr} + K_{R2zr}e^{-\beta h_1} + K_{R3zr}e^{-\beta h_2}\right), \quad S_8 = \frac{\mu_0}{2\beta}\left(K_{R1zi} + K_{R2zi}e^{-\beta h_1} + K_{R3zi}e^{-\beta h_2}\right). \quad (A.16)$$

The relationship between $\tilde{A}$ and $\tilde{H}$ is

$$H_x = \frac{1}{\mu_0}\frac{\partial A_z}{\partial y}, \qquad H_y = \frac{1}{\mu_0}\left(\frac{\partial A_x}{\partial z} - \frac{\partial A_z}{\partial x}\right), \text{ and } \qquad H_z = \frac{-1}{\mu_0}\frac{\partial A_x}{\partial y}. \tag{A.17}$$

Finally, the three components of $\tilde{H}$ at different layers can be expressed in the complete form:

$$(H_x)_{y=0} = \sum_{n=1}^{N}\sum_{m=1}^{M} \alpha\left(- A_{R1rmn} - A_{R2rmn}e^{\beta h_1} - A_{R3rmn}e^{\beta h_2} + A_{Srmn}e^{-\beta h}\right)\cos(\alpha x)\sin(\gamma z) - \alpha\left(A_{R1imn} + A_{R2imn}e^{\beta h_1} + A_{R3imn}e^{\beta h_2}\right)\sin(\alpha x)\sin(\gamma z), \tag{A.18a}$$

$$(H_y)_{y=0} = \sum_{n=1}^{N}\sum_{m=1}^{M} \beta\left(A_{R1rmn} + A_{R2rmn}e^{\beta h_1} + A_{R3rmn}e^{\beta h_2} + A_{Srmn}e^{-\beta h}\right)\sin(\alpha x)\sin(\gamma z) + \beta\left(A_{R1imn} + A_{R2imn}e^{\beta h_1} + A_{R3imn}e^{\beta h_2}\right)\cos(\alpha x)\sin(\gamma z), \tag{A.18b}$$

$$(H_z)_{y=0} = \sum_{n=1}^{N}\sum_{m=1}^{M} \gamma\left(- A_{R1rmn} - A_{R2rmn}e^{\beta h_1} - A_{R3rmn}e^{\beta h_2} + A_{Srmn}e^{-\beta h}\right)\sin(\alpha x)\cos(\gamma z) - \gamma\left(A_{R1imn} + A_{R2imn}e^{\beta h_1} + A_{R3imn}e^{\beta h_2}\right)\cos(\alpha x)\cos(\gamma z), \tag{A.18c}$$

$$(H_x)_{y=h_1} = \sum_{n=1}^{N}\sum_{m=1}^{M} \alpha\left(- A_{R2rmn} - A_{R3rmn}e^{\beta(h_2-h_1)} + A_{R1rmn}e^{\beta h_1} + A_{Srmn}e^{-\beta h+\beta h_1}\right)\cos(\alpha x)\sin(\gamma z) - \alpha\left(A_{R2imn} + A_{R3imn}e^{\beta(h_2-h_1)} - A_{R1imn}e^{\beta h_1}\right)\sin(\alpha x)\sin(\gamma z), \tag{A.19a}$$

$$(H_y)_{y=h_1} = \sum_{n=1}^{N}\sum_{m=1}^{M} \beta\left(A_{R2rmn} + A_{R3rmn}e^{\beta(h_2-h_1)} + A_{R1rmn}e^{\beta h_1} + A_{Srmn}e^{-\beta h+\beta h_1}\right)\sin(\alpha x)\sin(\gamma z) + \beta\left(A_{R2imn} + A_{R3imn}e^{\beta(h_2-h_1)} + A_{R1imn}e^{\beta h_1}\right)\cos(\alpha x)\sin(\gamma z), \tag{A.19b}$$

$$(H_z)_{y=h_1} = \sum_{n=1}^{N}\sum_{m=1}^{M} \gamma\left(- A_{R2rmn} - A_{R3rmn}e^{\beta(h_2-h_1)} + A_{R1rmn}e^{\beta h_1} + A_{Srmn}e^{-\beta h+\beta h_1}\right)\sin(\alpha x)\cos(\gamma z) - \gamma\left(A_{R2imn} + A_{R3imn}e^{\beta(h_2-h_1)} - A_{R1imn}e^{\beta h_1}\right)\cos(\alpha x)\cos(\gamma z), \tag{A.19c}$$

$$(H_x)_{y=h_2} = \sum_{n=1}^{N}\sum_{m=1}^{M} \alpha\left(- A_{R3rmn} + A_{R2rmn}e^{\beta(h_2-h_1)} + A_{R1rmn}e^{\beta h_2} + A_{Srmn}e^{-\beta h+\beta h_2}\right)\cos(\alpha x)\sin(\gamma z) + \alpha\left(- A_{R3imn} + A_{R2imn}e^{\beta(h_2-h_1)} + A_{R1imn}e^{\beta h_2}\right)\sin(\alpha x)\sin(\gamma z), \tag{A.20a}$$

$$(H_y)_{y=h_2} = \sum_{n=1}^{N}\sum_{m=1}^{M} \beta\left(A_{R3rmn} + A_{R2rmn}e^{\beta(h_2-h_1)} + A_{R1rmn}e^{\beta h_2} + A_{Srmn}e^{-\beta h+\beta h_2}\right)\sin(\alpha x)\sin(\gamma z) + \beta\left(A_{R3imn} + A_{R2imn}e^{\beta(h_2-h_1)} + A_{R1imn}e^{\beta h_2}\right)\cos(\alpha x)\sin(\gamma z), \tag{A.20b}$$

and

$$(H_z)_{y=h_2} = \sum_{n=1}^{N}\sum_{m=1}^{M} \gamma\left(- A_{R3rmn} + A_{R2rmn}e^{\beta(h_2-h_1)} + A_{R1rmn}e^{\beta h_2} + A_{Srmn}e^{-\beta h+\beta h_2}\right)\sin(\alpha x)\cos(\gamma z) + \gamma\left(- A_{R3imn} + A_{R2imn}e^{\beta(h_2-h_1)} + A_{R1imn}e^{\beta h_2}\right)\cos(\alpha x)\cos(\gamma z). \tag{A.20c}$$

The above can also be written as complex forms:

$$(H_y)_{y=0} = \text{Real}\sum_{n=1}^{N}\sum_{m=1}^{M} 0.5\beta\left(A_{R1mn} + A_{R2mn}e^{\beta h_1} + A_{R3mn}e^{\beta h_2} + A_{Smn}e^{-\beta h}\right) \times \left(e^{j(\alpha x+\gamma z)} - e^{j(\alpha x-\gamma z)}\right)$$

$$= H_{S1y} + H_{R11y} + H_{R12y} + H_{R13y}\,, \qquad \text{(A.21a)}$$

$$(H_y)_{y=h_1} = \text{Real}\sum_{n=1}^{N}\sum_{m=1}^{M} 0.5\beta\left(A_{R2mn} + A_{R3mn}e^{\beta(h_2-h_1)} + A_{R1mn}e^{\beta h_1} + A_{Smn}e^{-\beta h+\beta h_1}\right) \times \left(e^{j(\alpha x+\gamma z)} - e^{j(\alpha x-\gamma z)}\right)$$

$$= H_{S2y} + H_{R21y} + H_{R22y} + H_{R23y}\,, \qquad \text{(A.21b)}$$

and

$$(H_y)_{y=h_2} = \text{Real}\sum_{n=1}^{N}\sum_{m=1}^{M} 0.5\beta\left(A_{R3rmn} + A_{R2rmn}e^{\beta(h_2-h_1)} + A_{R1rmn}e^{\beta h_2} + A_{Srmn}e^{-\beta h+\beta h_2}\right) \times \left(e^{j(\alpha x+\gamma z)} - e^{j(\alpha x-\gamma z)}\right)$$

$$= H_{S3y} + H_{R31y} + H_{R32y} + H_{R33y}\,. \qquad \text{(A.21c)}$$

The form of H_x and H_z are similar.

If more layers are required to obtain higher accuracy, the derivations of H are similar to the above. The formula of H for NL layers should be

$$H_{kx} = H_{Skx} + \sum_{j=1}^{NL} H_{Rkjx} \quad (k = 1,2,..., NL)\,, \qquad \text{(A.22a)}$$

$$H_{ky} = H_{Sky} + \sum_{j=1}^{NL} H_{Rkjy} \quad (k = 1,2,..., NL)\,, \qquad \text{(A.22b)}$$

and

$$H_{kz} = H_{Skz} + \sum_{j=1}^{NL} H_{Rkjz} \quad (k = 1,2,..., NL)\,. \qquad \text{(A.22c)}$$

A.2 Guideway Modeling

This and the following sections follow the calculation of Ooi and Eastham (1975) but incorporate multiple layers in the guideway. To consider the finite width of the guideway, they described the sheet current in the guideway in the following form:

$$K_R = \text{Real Curl } \tilde{U}_y \; C(x,z) \,, \tag{A.23}$$

where

$$C(x,z) = \sum_{m=1}^{M} \sum_{l=1}^{2L-1} C_{ml} S_n \left(e^{j(\alpha x + \xi(z-D)} - e^{j(\alpha x - \xi(z-D))} \right) , \tag{A.24}$$

where $\xi = \pi l/d$ (d is the width of the guideway), l = 1,3,5... 2L-1, and S_n is the sign. For the region $(W/4 - d/2) \le z \le (W/4 + d/2)$, $S_n = 1$ and $D = W/4 - d/2$. For the region $(-W/4 - d/2) \le z \le (-W/4 + d/2)$, $S_n = -1$ and $D = -W/4 + d/2$. C_{ml} are the unknown complex coefficients to be solved. In other words, C(x,z) is represented by 2L-1 harmonics and is only valid in the guideway regions. When the guideway is divided into NL layers, then

$$C(x,z)_k = \sum_{m=1}^{M} \sum_{l=1}^{2L-1} C_{kml} S_n \left(e^{j(\alpha x + \xi(z-D)} - e^{j(\alpha x - \xi(z-D))} \right) \quad (k = 1,2,..., NL). \tag{A.25}$$

$C(x,z)_k$ can also be represented in the same double-Fourier series base as Equation A.21.

$$C(x,z)_k = \sum_{m=1}^{M} \sum_{n=1}^{N} \left(A_{Rkmn} e^{j(\alpha x + \gamma z)} + B_{Rkmn} e^{j(\alpha x - \gamma z)} \right) \quad (k = 1,2,..., NL) \tag{A.26}$$

Expanding Equation A.24 in the Fourier series base of Equation A.25, one can obtain the Fourier coefficients:

$$A_{Rkmn} = \sum_{l=1}^{2L-1} j2 \sin(\gamma W/4)(Y_l R_l - Z_l S_l) \; C_{kml} \quad (k = 1,2,..., NL) \,, \tag{A.27a}$$

and

$$B_{Rkmn} = -A_{Rkmn} \quad (k = 1,2,..., NL) \,, \tag{A.27b}$$

where

$$Y_l = e^{j\xi d/2} \,, \qquad Z_l = e^{-j\xi d/2} \,,$$

$$R_l = \frac{\sin\left((\xi + \gamma)d/2\right)}{(\xi + \gamma)W/2}, \qquad \text{and} \qquad S_l = \frac{\sin\left((\xi - \gamma)d/2\right)}{(\xi - \gamma)W/2}. \tag{A.28}$$

In order to implement an algorithm easily, one can define a NL*(2N) vector $\bar{A}_{Rm}$ containing A_{Rkmn} and B_{Rkmn} (k = 1,2,..., NL) and define a NL*(2N) base vector $\bar{b}_m$ containing $e^{j(\alpha x+\gamma z))}$ and $e^{j(\alpha x-\gamma z))}$. Equation A.26 can be rewritten as

$$C(x,z) = \sum_{m=1}^{M} \bar{b}_m^T \bar{A}_{Rm} . \tag{A.29}$$

The superscript T denotes the transpose of the vector.

An L vector $\bar{C}_{ml}$ can also be defined containing C_{kml} as following:

$$\bar{A}_{Rm} = \begin{bmatrix} [ARCL] & & & \\ & [ARCL] & & \\ & & \cdots & \\ & & & [ARCL] \end{bmatrix} \bar{C}_{ml} , \tag{A.30}$$

where [ARCL] is a $2N \times L$ matrix, whose elements are defined by Equations A.26 and A.27.

A.3 Guideway Interactions

Assume the guideway is divided into NL layers. In the region of the guideway, the relationship between the eddy current $\tilde{K}_{Rk}$ (k=1,2,...NL) and the electric field density $\tilde{E}_k$ (k=1,2,...NL) is

$$\tilde{K}_{Rk} = \sigma\, t_k\, \tilde{E}_k \qquad (k = 1,2,..., NL) , \tag{A.31}$$

where σ is the conductivity of the guideway, and t_k is the effective thickness of the guideway for the kth layer.

The electric field density $\tilde{E}_j$ can be written

$$\tilde{E}_k = \left(\tilde{v} \times \mu_0 \left(\tilde{H}_{Sk} + \sum_{j=1}^{NL} \tilde{H}_{Rkj} \right) - \text{grad}\, \Phi_k \right) \quad k = 1,2,..., NL . \tag{A.32}$$

where -grad Φ_k is the conservative electric field, and Φ_k satisfies div grad $\Phi_k = 0$. Φ_k can be written in a double-Fourier series:

$$\Phi_k = \text{Real} \sum_{m=1}^{M} \sum_{n=1}^{N} P_{kmn} e^{j(\alpha x+\gamma z)} + Q_{kmn} e^{j(\alpha x-\gamma z)} \quad (k = 1,2,..., NL). \tag{A.33}$$

Since $\tilde{K}_{Rk}$ only has x- and z-components, so does $\tilde{E}_k$., and since $\tilde{v} = v_x$. Equation A.32 becomes

$$E_{kx} = -\frac{\partial \Phi_k}{\partial x} \quad (k = 1, 2,..., NL), \tag{A.34}$$

and

$$E_{kz} = v_x \mu_0 \left(H_{Sky} + \sum_{j=1}^{NL} H_{Rkjy} \right) - \frac{\partial \Phi_k}{\partial z} \quad (k = 1,2,..., NL). \tag{A.35}$$

Note that Equation A.31 is valid only in the region of the guideway. This can be obtained by insisting that the following equation hold:

$$\sigma t_k \tilde{E}_k \cdot \tilde{K}_{Rk} = \tilde{K}_{Rk} \cdot \tilde{K}_{Rk} \quad (k = 1,2,... NL) , \tag{A.36}$$

in the surface integral over a Fourier period. Using the power equality equation, which is equivalent to saying that real and reactive powers in $|I|^2 Z$ are equal to these in $I E^*$, the following equations must be satisfied:

$$\int_{-L/2}^{L/2} \int_{-W/2}^{W/2} \left(\sigma t_k E_{kx} K_{Rkx} - K_{Rkx}^2 \right) dz\, dx = 0 \quad (k = 1,2,..., NL) , \tag{A.37}$$

and

$$\int_{-L/2}^{L/2} \int_{-W/2}^{W/2} \left(\sigma t_k E_{kz} K_{Rkz} - K_{Rkz}^2 \right) dz\, dx = 0 \quad (k=1,2,..., NL) . \tag{A.38}$$

From Equations A.23 and A.26, one can obtain

$$K_{Rkx} = \text{Real} \sum_{m=1}^{M} \sum_{n=1}^{N} j\gamma \left(A_{Rkmn} e^{j(\alpha x+\gamma z)} - B_{Rkmn} e^{j(\alpha x-\gamma z)} \right) \quad (k = 1,2..., NL), \tag{A.39}$$

and

$$K_{Rkz} = \text{Real} \sum_{m=1}^{M} \sum_{n=1}^{N} j\alpha \left(A_{Rkmn} e^{j(\alpha x+\gamma z)} + B_{Rkmn} e^{j(\alpha x-\gamma z)} \right) \quad (k = 1,2,.., NL). \tag{A.40}$$

Substituting Equations A.34 and A.39 into Equation A.37, one has the results:

$$P_{kmn} = \frac{\gamma A_{Rkmn}}{\alpha \sigma t_k} \quad (k = 1,2,..., NL), \tag{A.41}$$

and

$$Q_{kmn} = -\frac{\gamma B_{Rkmn}}{\alpha \sigma t_k} \quad (k = 1,2,..., NL). \tag{A.42}$$

Using the 2N vector $\bar{b}_{km}$ (k = 1,2,..., NL) as base, H_{Sky} and $\sum_{j=1}^{NL} H_{Rkjy}$ (k = 1,2,..., NL) in Equation A.22 can be written as

$$H_{Sky} = \text{Real} \sum_{m=1}^{M} \bar{b}_{km}^T \bar{H}_{Skm} \quad (k = 1,2,..., NL), \tag{A.43}$$

and

$$H_{Rkjy} = \text{Real} \sum_{m=1}^{M} \bar{b}_{km}^T \bar{H}_{Rkjm} \quad (k, j = 1,2,..., NL). \tag{A.44}$$

where

$$\bar{H}_{Skm} = [HSAS_k] \bar{A}_{Skm} \quad (k = 1,2,..., NL), \tag{A.45}$$

and

$$\begin{aligned} \bar{H}_{Rkjm} &= [HRAR_{kj}] \bar{A}_{Rkjm} = [HRAR_{kj}] [ARCL] \bar{C}_{kml} \\ &= [HRCL_{kj}] \bar{C}_{kml} \quad (k,j = 1,2,..., NL). \end{aligned} \tag{A.46}$$

Likewise, the z-component of $\tilde{K}_{Rk}$ and $\tilde{E}_{Rk}$ can be written as

$$K_{Rkz} = \text{Real} \sum_{m=1}^{M} \bar{b}_{km}^T \bar{K}_{kzm} \quad (k = 1,2,..., NL), \tag{A.47}$$

and

$$E_{kz} = \text{Real} \sum_{m=1}^{M} \bar{b}_{km}^T \bar{E}_{kzm} \quad (k = 1,2,..., NL). \tag{A.48}$$

From Equations A.25 and A.26, one has

$$\overline{K}_{kzm} = [KZCL_k]\,\overline{C}_{kml} \quad (k = 1,2,..., NL)\ . \tag{A.49}$$

From Equation A.35, one has

$$\overline{E}_{kzm} = \mu_0\, v\left(\overline{H}_{Skm} + \sum_{j=1}^{NL} \overline{H}_{Rkjm}\right) + [EZPQ_k]\,\overline{P}_{km}$$

$$= \mu_0\, v\,[HSAS_k]\,\overline{A}_{Skm} + \mu_0\, v \sum_{j=1}^{NL} [HRCL_{kj}]\,\overline{C}_{kml}$$

$$+ [EZPQ_k]\,\overline{P}_{km} \quad (k = 1,2,..., NL)\ , \tag{A.50}$$

where $\overline{P}_{km}$ is a 2N vector containing the coefficients P_{kmn} and Q_{kmn} in Equation A.33. Equations A.41 and A.42 can be written as

$$\overline{P}_{km} = [PQAR_k]\,\overline{A}_{Rkm} = [PQAR_k][ARCL]\,\overline{C}_{kml} \quad (k = 1,2,..., NL) \tag{A.51}$$

Substituting Equation A.51 into Equation A.56 and thereafter Equations A.49 and Equations A.50 into A.38, one has

$$\sum_{m=1}^{M} \overline{C}^{*T}_{ml} \left\{[Z_m]\,\overline{C}_{ml} - [Y_m]\,\overline{A}_{Sm}\right\} = 0\ ,$$

where * denotes the complex conjugate operation, and

$$[Z_m] = \begin{bmatrix} [Z_{11m}] & [Z_{12m}] & \cdots & [Z_{1NLm}] \\ [Z_{21m}] & [Z_{22m}] & \cdots & [Z_{2NLm}] \\ & \ddots & & \\ [Z_{NL1m}] & [Z_{NL2m}] & \cdots & [Z_{NLNLm}] \end{bmatrix}, \text{ and } [Y_m] = \begin{bmatrix} [Y_{1m}] \\ [Y_{2m}] \\ \vdots \\ [Y_{NLm}] \end{bmatrix}, \tag{A.52}$$

where

$$[Z_{11m}] = [KZCL_1]^{*T}\{\sigma\, t_1\, \mu_0\, v\,[HRCL_{11}] + \sigma\, t_1\,[EZPQ_1][PQCL_1] - [KZCL_1]\}\ ,$$

$$[Z_{12m}] = [KZCL_1]^{*T}\{\sigma\, t_1\, \mu_0\, v\,[HRCL_{12}]\}\ ,$$

$$\vdots$$

$$[Z_{1NLm}] = [KZCL_1]^{*T}\{\sigma\, t_1\, \mu_0\, v\, [HRCL_{1NL}]\}\,,$$

$$[Z_{21m}] = [KZCL_2]^{*T}\{\sigma\, t_2\, \mu_0\, v\, [HRCL_{21}]\}\,,$$

$$[Z_{22m}] = [KZCL_2]^{*T}\{\sigma\, t_2\, \mu_0\, v\, [HRCL_{22}] + \sigma\, t_2\, [EZPQ_2]\,[PQCL_2] - [KZCL_2]\}\,,$$

$$\vdots$$

$$[Z_{2NLm}] = [KZCL_2]^{*T}\{\sigma\, t_2\, \mu_0\, v\, [HRCL_{2NL}]\}\,,$$

$$[Z_{NL1m}] = [KZCL_{NL}]^{*T}\{\sigma\, t_{NL}\, \mu_0\, v\, [HRCL_{NL1}]\}\,,$$

$$[Z_{NL2m}] = [KZCL_{NL}]^{*T}\{\sigma\, t_{NL}\, \mu_0\, v\, [HRCL_{NL2}]\}\,,$$

$$\vdots$$

$$[Z_{NLNLm}] = [KZCL_{NL}]^{*T}\left\{\begin{array}{c}\sigma\, t_{NL}\, \mu_0\, v\, [HRCL_{NL}] + \\ \sigma\, t_{NL}\, [EZPQ_{NL}]\,[PQCL_{NL}] - [KZCL_{NL}]\end{array}\right\}\,,$$

$$[Y_{1m}] = [KZCL_1]^{*T}\{-\sigma\, t_1\, \mu_0\, v\, [HSAS_1]\}\,,$$

$$[Y_{2m}] = [KZCL_2]^{*T}\{-\sigma\, t_2\, \mu_0\, v\, [HSAS_2]\}\,,$$

$$\vdots$$

$$[Y_{NLm}] = [KZCL_{NL}]^{*T}\{-\sigma\, t_{NL}\, \mu_0\, v\, [HSAS_{NL}]\}\,,$$

$[Z_m]$ is a (NL)L × (NL)L matrix and $[Y_m]$ is a (NL)L × (NL) 2N matrix. Equation A.38 is satisfied only when

$$\overline{C}_{ml} = [Z_m]^{-1}[Y_m]\,\overline{A}_{Sm}\,. \tag{A.53}$$

A.4 Electromechanical Forces

The Lorentz force law $\tilde{J} \times \tilde{B}$ can be applied to the guideway. The lift force F_y and the drag force F_x are

$$F_y = \frac{1}{4}\sum_{k=1}^{NL} \int_{-L/2}^{L/2} \int_{-w/2}^{w/2} -\mu_0 \left(K_{Rkz}\, H_{Skx} - K_{Rkx}\, H_{Skz}\right) dx\, dz$$

$$= \frac{1}{4}\sum_{k=1}^{NL} \text{Real}\left(0.5\,\mu_0\, LW \sum_{m=1}^{M}\sum_{n=1}^{N} 0.5\,\beta^2\, e^{-\beta h_k}\left(A^*_{Rkmn}\, A_{Skmn} + B^*_{Rkmn}\, B_{Skmn}\right)\right), \quad \text{(A.54)}$$

where h_k is the distance between the magnet and the kth sheet current of the guideway.

$$F_x = \frac{1}{4}\sum_{k=1}^{NL} \int_{-L/2}^{L/2} \int_{-w/2}^{w/2} \mu_0\, K_{Rkz}\, H_{Sky}\, dx\, dz$$

$$= \frac{1}{4}\sum_{k=1}^{NL} \text{Real}\left(0.5\,\mu_0\, LW \sum_{m=1}^{M}\sum_{n=1}^{N} 0.5\,\alpha\,\beta\, e^{-\beta h_k}\left(jA)^*_{Rkmn}\, A_{Skmn} + (jB)^*_{Rkmn}\, B_{Skmn}\right)\right). \quad \text{(A.55)}$$

There is no guidance force unless the magnet is laterally displaced. Figure A.3 shows that the magnet is laterally displaced by z_0. In this case, the vector $\bar{A}_{Sm}$ contains a new set of Fourier coefficients:

$$A^g_{Skmn} = A_{Skmn} e^{-j\gamma z_0} \qquad \text{and} \qquad B^g_{Skmn} = B_{Skmn} e^{j\gamma z_0}\ .$$

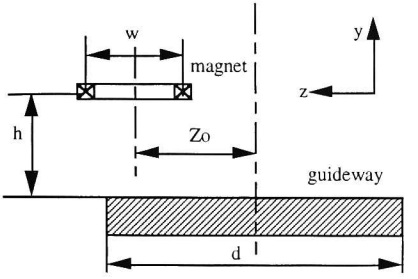

FIGURE A.3 Magnet at Transverse Displacement z_0 from Guideway Centerline

The expression of guideway current in Equation A.25 keeps same except that l = 1,2,3,4,.. 2L, i.e., both odd and even harmonics exist. The guidance force is

$$F_z = \frac{1}{4}\sum_{k=1}^{N_L} \int_{-L/2}^{L/2} \int_{-W/2}^{W/2} \mu_0 \, K_{Rkx} \, H_{Sky} \, dx \, dz$$

$$= \frac{1}{4}\sum_{k=1}^{N_L} \text{Real}\left(0.25 \, \mu_0 \, LW \sum_{m=1}^{M} \sum_{n=1}^{N} j \, \gamma \, \beta \, e^{-\beta h} \left((-A)^*_{Rkmn} \, A^g_{Skmn} + (B)^*_{Rkmn} \, B^g_{Skmn} \right) \right) . \quad (A.56)$$

Appendix B:

Errors in the Ooi and Eastham (1975) Paper and the Ooi (1975) Paper

Appendix B:

Errors in the Ooi and Eastham (1975) Paper and the Ooi (1975) Paper

PAPER: Ooi and Eastham 1975.

Equation 1 should be

$$\widetilde{K}_S = \text{Real Curl } \widetilde{U}_y \sum \left(A_{Smn}\, e^{j(\alpha x + \gamma z)} + B_{Smn}\, e^{j(\alpha x - \gamma z)} \right) \tag{1}$$

Equation 2 should be

$$A_{Smn} = \frac{AT}{nm} \frac{8}{\pi^2} \sin\left(\frac{n\pi}{2}\right) \sin\left(\frac{m\pi}{2}\right) \sin\left(\frac{n\pi w}{W}\right) \sin\left(\frac{n\pi l}{L}\right) \tag{2}$$

Equation 7 should be

$$A_{rmn} = \sum_{l=1}^{2L-1} j2 \sin(\gamma W/4)(Y_l R_l - Z_l S_l) \tag{7}$$

Equations 22 and 23 should be

$$F_y = \frac{1}{4} \int_{-L/2}^{L/2} \int_{-W/2}^{W/2} - \mu_0 \left(K_{rz}\, H_{sx} - K_{rx}\, H_{sz}\right) dx\, dz$$

$$= \frac{1}{4} \text{Real} \left(0.5\, \mu_0\, LW \sum 0.5\, \beta^2\, e^{-\beta h} \left(A^*_{rmn}\, A_{smn} + B^*_{rmn}\, B_{smn} \right) \right) \tag{22}$$

$$F_x = \frac{1}{4} \int_{-L/2}^{L/2} \int_{-W/2}^{W/2} \mu_0\, K_{rz}\, H_{sy}\, dx\, dz$$

$$= \frac{1}{4} \text{Real} \left(0.5\, \mu_0\, LW \sum 0.5\, \alpha\, \beta\, e^{-\beta h} \left((jA)^*_{rmn}\, A_{smn} + (jB)^*_{rmn}\, B_{smn} \right) \right) \tag{23}$$

PAPER: Ooi 1975:

Equation 7 should be

$$F_z = \frac{1}{4}\int_{-L/2}^{L/2}\int_{-w/2}^{w/2} \mu_0 K_{rx} H_{sy}\, dx\, dz$$

$$= \frac{1}{4}\text{Real}\left(0.25\,\mu_0 LW \sum j\,\gamma\,\beta\, e^{-\beta h}\left((-A)^*_{rmn} A^1_{smn} + (B)^*_{rmn} B^1_{smn}\right)\right) \quad (7)$$

Equations 9a and 9b should be

$$A^{11}_{smn} = -2\, j\sin\left(\frac{\gamma C_z}{2}\right) e^{-j\gamma z_0} A_{smn} \quad (9a)$$

$$B^{11}_{smn} = 2\, j\sin\left(\frac{\gamma C_z}{2}\right) e^{-j\gamma z_0} B_{smn} \quad (9b)$$